

Four years of active sampling of atmospheric polycyclic aromatic hydrocarbons (PAHs) and oxygenated PAHs in Dronning Maud Land, East Antarctica

Preben Van Overmeiren^{a,*}, Patrick De Wispelaere^a, Kristof Demeestere^a, Stefania Gili^{b,c}, Alexander Mangold^d, Karen De Causmaecker^d, Nadine Matielli^b, Andy Delcloo^{d,e}, Herman Van Langenhove^a, Christophe Walgraeve^a

^a Research group EnVOC (Environmental Organic Chemistry and Technology), Department of Green Chemistry and Technology, Faculty of Bioscience Engineering, Ghent University, Ghent, Belgium

^b G-Time Laboratory, Département des Géosciences, Environnement et Société, Université Libre de Bruxelles, Brussels, Belgium

^c Now at The Higgins Research Laboratory, The Higgins Research Laboratory, Princeton University, Princeton, NJ, USA

^d Royal Meteorological Institute of Belgium (RMI), Ukkel, Belgium

^e Department of Physics and Astronomy, Ghent University, Ghent, Belgium

*Corresponding author: Preben Van Overmeiren (preben.van.overmeiren@ugent.be), Coupure Links 653, Ghent, Belgium

To be submitted in;

- Environmental science and technology (11.36) – Q1 (7000 words equivalents)
200 words for each small figure, scheme, or table that takes up part of a page. Large multipart figures, extensive tables, detailed maps, or chemical pathways taking up a page or more should be counted as 600 words. At the discretion of the assigned editor, some figures or tables may be counted as more than 600 words

Highlights

Abstract

1 Introduction

Polycyclic aromatic hydrocarbons (PAHs) are a large group of semi-volatile organic pollutants sharing the same chemical backbone. They are composed of solely carbon and hydrogen and contain at least 2 fused aromatic rings, making them the most stable hydrocarbons. Incomplete combustion, pyrolysis of fossil fuels and wood, and petroleum products are amongst the main anthropogenic sources which predominate compared to natural sources such as volcanic activity. To limit the analytical complexity and to improve consistency and comparability across datasets, the U.S. Environmental Protection Agency (EPA) issued a list of 16 ‘priority PAHs’ in 1976 which have been the subject of environmental analysis and monitoring ever since (Andersson and Achten, 2015). PAHs are ubiquitous in the atmosphere, either in the gaseous phase or associated to particles, which is a cause of concern. With benzo[*a*]pyrene being a notable example, many PAHs are classified as known carcinogens to biota (World Health Organisation, 2021). Furthermore, they are known to be transported over long distances, making them a concerning class of persistent organic pollutants (POPs). This brought the United Nations Economic Commission for Europe’s (UNECE) to incorporate PAHs in the Convention on Long-range Transboundary Air Pollution (CLRTAP) (UNECE, 1998). Although the emission of PAHs is reported to be decreasing, with an estimated 470 Gg (16 EPA PAHs) emitted globally in 2014 (Li et al., 2022), it comes to no surprise that they are found at low levels (pg m⁻³ levels) even in the most remote regions of the world (Cabrerizo et al., 2014; Friedman and Selin, 2012). Long-range atmospheric transport (LRAT) has been reported as the most efficient way for PAHs emitted from lower latitudes to reach the polar regions.

Because of the broad range of vapor pressures (11.3 to 1.33×10^{-8} Pa at 25°C for naphthalene and benzo[ghi]perylene), which decreases with the number of aromatic rings, a distribution between the gas phase and particulate matter (PM) phase takes place for each compound. Compounds with 5 or more rings are, at atmospheric temperatures, typically sorbed to PM leading to lower mobility. PAHs with a lower molecular weight (LMW) (≤ 202 g/mol) partition between the gas and particle phase and can undergo worldwide dispersion (Bidleman, 1988; Ravindra et al., 2008). This results in low molecular weight (LMW) PAHs being dominant in remote regions (Na et al., 2020; Yang et al., 2016).

Besides LRAT other sources to consider specifically for Antarctica are the revolatilization from surface snow and soil (Cabrerizo et al., 2014) and the Antarctic Ocean via air-seawater exchange (Cao et al., 2018). Both can contribute to the level of 3 and 4 ring PAHs, especially with elevated temperatures during the summer. Local pollution caused by research and tourism is receiving increasing attention as another source of PAHs in Antarctica (Kukučka et al., 2010; Yao et al., 2016).

Compared to other POPs such as PCBs, the atmospheric lifetimes of PAHs in the gas phase are limited, between a few hours and days. However, when associated to particles the atmospheric lifetimes increase significantly making them stable enough to undergo LRAT (Keyte et al., 2013; Lohmann et al., 2009). During this LRAT PAHs react with $\cdot\text{OH}$ radicals and ozone, forming oxygenated PAHs (oxy-PAHs). As defined by (Walgraeve et al., 2017) oxy-PAHs are ketones and quinones of PAHs and thus contain at least one carbonylic oxygen. Oxy-PAHs are more polar and typically have a lower vapor pressure, resulting in a higher tendency to be associated with PM, and are characterized by a stronger toxic effect because of the direct mutagenic potency compared to their parent PAHs (Clergé et al., 2019; Lundstedt et al., 2007; Walgraeve et al., 2010).

To determine atmospheric concentrations of both PAHs and oxy-PAHs in remote environments (pg m^{-3} range), typically a high-volume sampler (HVS) is used. This sampler collects PM on a glass (GFF) or quartz (QFF) fiber filter but can be augmented with a polyurethane filter (PUF) to simultaneously collect gaseous PAHs. Soxhlet extraction used to be the extraction method of choice for these sample media but pressurized liquid extraction (PLE) and ultrasonic extraction (USE) quickly caught up showing excellent extraction efficiencies for both PAHs and oxy-PAHs (He and Balasubramanian, 2009; Walgraeve et al., 2015) while decreasing solvent usage fitting the green chemistry philosophy. Analysis traditionally takes place using a gas chromatograph coupled to a mass spectrometer (GC-MS) or high-performance liquid chromatography (HPLC) with a UV or fluorescence spectroscopy detector.

Legacy pollutants like organochlorine pesticides (OCPs) or PCBs are more regularly measured in the Antarctic atmosphere. In contrast, only 7 studies report PAH concentrations in the Antarctic lower atmosphere. Some clear knowledge gaps are identified in the existing literature. Previous studies on atmospheric PAHs in Antarctica deal with samples taken at the sea or at stations close to the ocean. As seawater-air exchange might be an important driver for PAH concentrations in remote oceanic areas, samples from further inland are possibly more influenced by atmospheric transport. A strong geographical focus lies on the Antarctic peninsula and Terra Nova Bay. While (Zhang et al., 2021) and (Cabrerizo et al., 2014) measured methylated PAHs as well as some sulfur- and nitrogen-containing PAHs, the main focus continues to lie on the 16 EPA PAHs. Oxy-PAHs were, to our knowledge, never measured in Antarctica.

The focus of this work is on the land based simultaneous sampling of both the gas and the particulate phase in Queen Maud Land, East-Antarctica to quantify the occurrence of both PAHs and oxy-PAHs in this remote atmosphere. With the support of dispersion analysis, we seek to identify events of LRAT and to better understand transformations and gas-particle partitioning in Antarctica.

2 Materials and Methods

2.1 Chemical standards and solvents

A mixture of the sixteen US-EPA PAHs (S.I. 1) in toluene with a concentration of 100 µg/mL each was purchased at Chiron AS, Norway, together with a mix of 7 perdeuterated PAHs (naphthalene-d8, biphenyl-d10, phenanthrene-d10, pyrene-d10, benzo[a]-pyrene-d10, benzo[a]-anthracene-d12 and benzo[ghi]-perylene-d12) (200-201 µg mL⁻¹ in toluene). A stock solution of 13 oxy-PAHs was made gravimetrically in toluene (1,4-Naphthalenedione, naphthalene-1-carboxaldehyde, 9-fluorenone, fluorene-2-carboxaldehyde, anthracene-9-one, anthracene-9,10-dione, 2-methylanthraquinone, 1,8-naphthalic anhydride, phenanthrene-9-carboxaldehyde, benzanthrone, pyrene-1-carboxaldehyde, benz[a]anthracene-7,12-dione, 5,12-naphthacenequinone) to obtain a concentration between 382 and 494 µg mL⁻¹. The pure compounds were obtained from Acros Organics (Belgium) or Sigma-Aldrich (Belgium). The exact composition of the used standards is given in S.I. 2 and S.I. 3. High purity n-hexane (Suprasolv®, hypergrade for organic trace analysis, Supelco, USA) and acetone (Distol®, for residue analysis, Fisher, USA) were used as extraction solvents. Toluene (Distol®, for residue analysis, Fisher, USA) was used as a solvent for the Oxy-PAH standards and for the final sample reconstitution. The purity of the used solvents was regularly tested by evaporating 100 mL of solvent to a volume of 1 mL and subsequently analyzing it. Nitrogen (Alfagaz 2, Air Liquide, France) was used as a purge gas. All standards, samples and stock solutions were stored at -21°C.

2.2 Sampling campaign

A Digital high-volume sampler (HVS), type DHA-80, obtained from Riemer Messtechnik, Germany, was installed in a measurement shelter in the vicinity of the Belgian Research Base, Princess Elisabeth Station (PEA) (71°57'S; 23°20'E), 1390 m a.s.l.) situated in the Dronning Maud Land region in East-Antarctica, ± 250 km from the grounding line (S.I. 4)(Figure 1). It was equipped with a filter holder for 150 mm quartz fiber filters (QFF) followed by a holder for a 6.0 x 7.6 cm polyurethane foam cartridge (PUF) to collect the particulate and gaseous phase separately. A PM₁₀ impactor inlet was used to avoid drifting snow entering the system. The impact on the measurement is negligible as (Herenz et al., 2019) proved that the expected particle size is a lot smaller than 10 µm. A 2D ultrasonic anemometer (Thies Clima, Germany) was used to activate the blower only when the wind speed was sufficiently high (at least 3 m.s⁻¹) and from the dominant wind direction window (125° ± 60°), to ensure sampling from a clean air sector. Sampling took place during the austral summers of 2017-2018, 2018-2019, 2019-2020 and 2020-2021. The maximum sample duration was set to 7 days (10080 minutes). However, as the HVS is turned off, or on, depending on the prevailing wind conditions, the actual sampling volume at standard conditions varies per sample. The sampling flow rate was set to 500 L min⁻¹. The sample volumes under standard conditions (298 K and 1013 hPa) were calculated from the total sample time and the standardized flow rate (Q_s) using the measured atmospheric pressure (p_m) and temperature (T_m) (equation S.I. 6). Field blanks were collected by inserting both filters in the sampler, turning the pump on, and turning it back off when the nominal sample flow rate of 500L/min was reached.

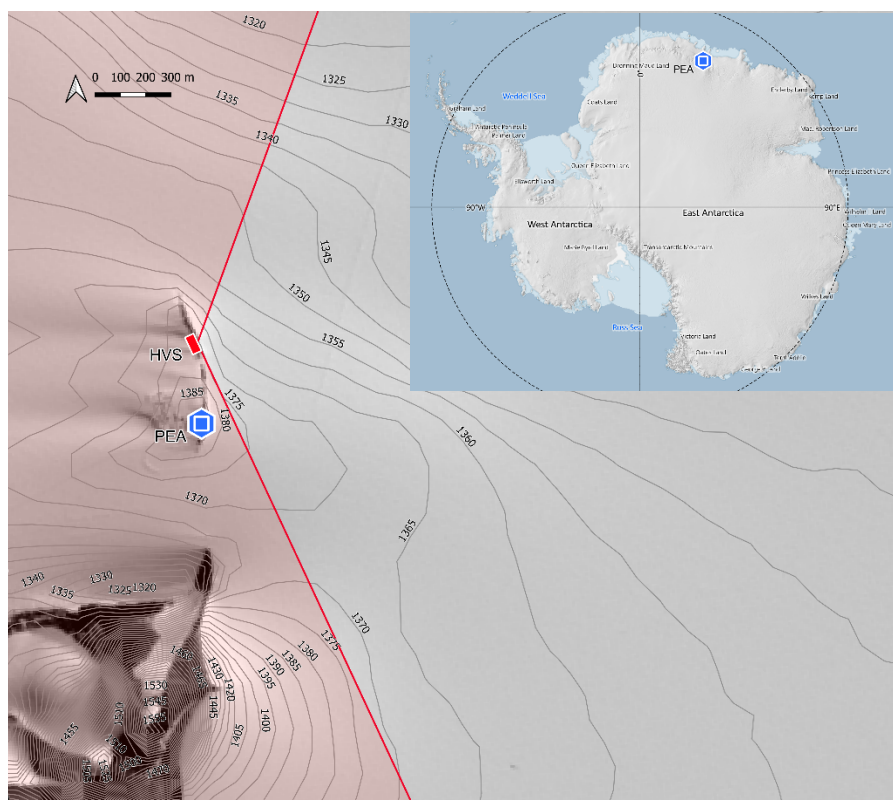


Figure 1: The sample location on the Utsteinen ridge (marked HVS), insert situating the Princess Elisabeth Antarctica (PEA) Station on the Antarctic continent. To only sample air from the clean air sector, the high-volume sampler is automatically switched off when wind is blowing from the red area. References; Quantartica (npolar.no), Sentinel (ESA), TanDEM-X (EOC Geoservice).

2.3 Sample preparation and extraction

All sample media were extracted using pressurized liquid extraction (PLE) using a Dionex ASE350 (Thermo Scientific, USA). In table 1 an overview is given of the used PLE programs. Details on the maintenance and cleaning of the ASE350 are in S.I. 5.

Table 1: Used PLE methods and corresponding parameters. Ex. methods indicate PLE methods used for the extraction of PUFs or QFF. Clean methods were used to clean the PUF before sampling. Cond. The method was used to condition the ASE cell to remove contaminations and reduce carry-over.

	Ex. 1 (Clean 2)	Ex. 2	Clean 1	Clean 3	Ex. 3	Ex. 4	Cond. 1
Cell Size	66 mL	66 mL	66 mL	66 mL	22 mL	22 mL	22 or 66 mL
Acetone:n-Hexane ratio (v/v)	25:75	25:75	50:50	0:100	25:75	25:75	50:50
Temperature	100°C	100°C	100°C	100°C	150°C	150°C	150°C
Heating time	5 min	5 min	5 min	5 min	7 min	7 min	7 min
Static time	5 min	5 min	5 min	5 min	5 min	5 min	5 min
Rinse	50%	50%	35%	35%	50%	50%	100%
Purge time	20	240	20	20	20	240	240
Glass microfiber filter	No	No	No	No	Yes	Yes	No
Solvent Saver	Yes	Yes	Yes	Yes	Yes	Yes	Yes

Prior to use, the PUFs (Orbo 2000, Supelco, 6.0 x 7.6 cm) were first removed from the glass holders and rinsed with demineralized water after which they were conditioned per 2 in the Zr cell using method Clean 1, Clean 2, and Clean 3 sequentially. The obtained extracts of each final cleaning step were analyzed to evaluate residual contaminations using the GC-HRMS method described in Section

2.4. The glass PUF holders were rinsed with acetone and n-hexane and dried at 200°C. The PUF's were, while still wet with hexane, re-inserted in the glass holders and blown dry with nitrogen. The cartridge was wrapped into aluminum foil and stored in a precleaned 1 L glass bottle (PTFE liner in cap) and purged with nitrogen.

The QFFs (Whatman QM-A, 150 mm, 2.20 µm pore size) were inserted in aluminum envelopes (20 cm x 20 cm, 100 µm thickness) and baked in a muffle furnace at 550 °C for 12 hours. They were transported to Antarctica in precleaned 1 L glass bottles. The thread of all sample bottles was wrapped with PTFE tape to improve the seal and a mark was added to detect tampering.

After sampling the QFF was re-inserted in its original aluminum envelope while the PUF cartridge was wrapped into clean aluminum foil. Both sampling media were stored together in 1 sample bottle. All samples were stored at -20°C and shipped in cold chain cargo.

At least twelve hours before extraction, the samples were removed from the freezer. Each PUF was extracted in a Zr cell at 100°C using method Ex 1, followed by Ex 2 (Table 1). The QFFs were cut into smaller pieces (1 to 2 cm²) and were extracted in SST cells at 150 °C using method Ex 3 two times followed by method Ex 4 (Table 1). To protect the stainless-steel frits of the cells from clogging, a small glass microfiber filter (Ahlstrom, Finland) (baked for 12 hours at 450°C) was inserted at the bottom of the SST cell when extracting QFFs. The extracts of two samples (01 Jan 2020 – 08 Jan 2020 and 22 Jan 2021 - 29 Jan 2021) were dried over a column filled with 5 g of MgSO₄ after they were found to be wet because of the intrusion of snow in the inlet during a storm. The extract's volume was reduced to the final droplet in a test-tube (20 mm x 150 mm, Pyrex, prebaked at 450°C for 12 hours) by evaporation using a gentle nitrogen stream in a concentrator station (Turbovap LV, Biotage). Immediately after the solvent reduction, 1 µL of the internal standard (D-PAHs, 200-201 ng) was added and the sample volume was reconstituted to 1 mL with toluene. The test tube was vortexed 2 times for 10 seconds. The contents were transferred to a 2 mL vial and stored at -21°C until GC-HRMS analysis (see Section 2.5). No blank correction was applied given the poor S/N ratio (< 3) of compounds in the method blanks and when S/N was sufficient, blank levels were low (< 5 %) compared to the sample. One notable exception is naphthalene for which a blank correction was applied.

2.4 GC-HRMS analysis

All samples were analyzed on a Trace GC (Thermo Finnigan, USA) coupled to a double sector high resolution (HR) mass spectrometer (MS) (Thermo Finnigan MAT95XP-TRAP, USA). A Rxi-17Sil MS column (30 m x 0.25 mm x 0.25 µm, Restek, USA) was used for separation, as this column has excellent selectivity for PAHs and low bleed. A guard column (deactivated fused silica, 0.25 mm I.D.) of 60 cm was installed in front of the GC column. The PAHs and oxy-PAHs were analyzed in 2 GC-MS runs in multiple ion detection (MID) mode, to increase the measurement time per ion. The MID windows for both methods are given in S.I. 9 and S.I. 10. Data were processed using Xcalibur 4.2 (Thermo Scientific) software.

2.5 Quality Control

Quality of the analysis was monitored to ensure results of different sampling seasons are intercomparable. A sequence of dilutions of the PAH standard mixture was used to create a calibration series from 1, 5, 10, 20, 50, 100 ng/mL. Each dilution was measured in threefold and the relative standard response factor for each compound is derived from the calibration curve. The instrument detection limit (IDL) is calculated from the relative standard deviation (RSD) on the 5 ng/mL point and the following formula: $IDL (ng) = t \times \frac{RSD_i}{100} \times 5 (ng)$ with RSD being the relative standard deviation (n=3) of compound I, and t a confidence factor determined using Student t-distribution with a 95 %

confidence level and 2 degrees of freedom. The intraday precision is determined on the repeated injection (n=4) of a 100 ng/mL standard solution, while the interday precision was calculated from the repeated injection of this standard over 4 days. Analog procedures were applied for the oxy-PAHs and the quality measures for both GC-HRMS methods are given in S.I. 11. The separation quality was determined qualitatively by interpreting the peak overlap of benzo[b]fluoranthene and benzo[k]fluoranthene. The method detection limit (MDL) and method quantification limit (MQL) were determined from the average of each compound i of the 6 field blanks (\overline{mass}_i) using the following formulae: $MDL_i = \overline{mass}_i + 3 \times SD_i \times V_{i,std}^{-1}$ and $MQL_i = \overline{mass}_i + 10 \times SD_i \times V_{i,std}^{-1}$ and are given in S.I. 17.

2.6 Positive Matrix Factorization (PMF) and dispersion modeling.

PMF (version 5.0) (Paatero and Tapper, 1994) was used on the total sample (PM + gas) to quantify the contribution of sources of PAHs and oxy-PAHs in Antarctica. The FLEXPART dispersion model (Stohl et al., 2005) was applied to identify potential source regions for the individual sample periods of the active sampling during seasons 2017/18 up to 2020/21. FLEXPART is a Lagrangian particle dispersion transport model which has originally been designed for calculating the long-range and mesoscale dispersion of air pollutants from point sources. FLEXPART was run 30 days back in time starting at the last day of each sample period, to 30 days before that day. The model was driven with ECMWF ERA5 meteorological fields (0.5° x 0.5° grid). Wet or dry deposition was not considered, and the model was run with passive tracers. The simulations include altitudes up to 10000 m a.g.l. In this way, the dispersion analysis yielded probability functions for the source regions and atmospheric pathways. The analysis gives thus a residence time, where the total is the sum over the whole simulation period. For a given location, the respective relative-to-the-total residence time can be derived and shown. It can be either summed over all or part of the vertical levels.

2.7 Meteorological data and total suspended particulate measurements

Atmospheric temperature and pressure were recorded by a weather station installed 2 km downwind from the sampling location. The station consists of 2 temperature probes (Young, U.S.A.) of which the data is averaged and a barometer (Young, U.S.A) connected to a Campbell Scientific datalogger. The station is maintained by the International Polar Foundation (IPF). During the 2018-19, 2019-20 and 2020-21 measurement a tapered element oscillating microbalance (TEOM) 1400ab equipped with a filter dynamics measurement system (TDMS) 8500 from Thermo Scientific was installed in a secondary measurement shelter to measure total suspended particulate concentrations (TSP). A 3 L/min flowrate was used, and data was reported hourly as a 24-hour running average. A precision of $\pm 0.5 \mu\text{g m}^{-3}$ is obtained. Values below $0 \mu\text{g m}^{-3}$ (sublimation or turbulent conditions) were removed from the dataset and the hourly data was averaged and corrected for the ambient temperature and air pressure over the total sample duration for each HVS sample.

3 Results and discussion

3.1 Analytical method development: analyte recovery

To determine the analyte recovery, three PUF filters were spiked with 1 µL of PAH standard solution, resulting in 100 ng of each PAHs, and 1 µL of a 1:10 dilution in toluene of the oxy-PAH stock solution, resulting in between 38 and 49 ng of oxy-PAHs on the filter. The PUFs were subsequently extracted, the extract concentrated, and solvent exchanged, and analyzed using the methodology described in Section 2.3 and 2.4. Recovery is calculated as per equation (1). Average analyte recoveries (S.I. 12) were obtained (between 74 and 143%) for all compounds except for naphthalene ($68 \pm 7 \%$), naphthalene-1,4-dione ($54 \pm 9 \%$) and Anthracen-9-one ($21 \pm 8 \%$).

$$Recovery_i(\%) = \frac{mass_{measured,i}}{mass_{spiked,i}} \times 100$$

(1)

To determine the analyte recovery from the QFF, they were loaded with ± 10 mg urban dust (NIST SRM 1649b) (weighed on an analytical balance - 0.01 mg resolution). More vigorous PLE parameters compared to the PUF extraction were evaluated, 3 extraction cycles at 125°C, 3 extraction cycles at 150°C and 3 extraction cycles at 150°C with the QFF cut into 2 cm² pieces. A disadvantage is that not all analytes are included in the certificate of SRM 1649b. For the 15 PAHs quantified in the certificate good recoveries between 52 and 142% were obtained for the latter method. For oxy-PAHs only information values are given. (Walgraeve et al., 2015) compiled other studies which quantified oxy-PAHs in the urban dust standard. The resulting recoveries (between 33 and 144 %) given in S.I. 12 are based on the levels of oxy-PAHs reported in this paper.

3.2 Occurrence of PAHs and oxy-PAHs in the atmosphere

A total of 32 samples were collected (between 6 and 10 weekly samples each summer) during the 4 year-long campaign. The average sample volume was 3456 m³. Of the 16 targeted EPA PAHs and the 13 oxy-PAHs on the target list, 15 PAHs and 12 oxy-PAHs were regularly detected and/or quantified. Dibenz[*a,h*]anthracene and 2-fluorene-carboxaldehyde remained under the detection limit for all samples. Atmospheric concentrations of PAHs and Oxy-PAHs are summarized in Figure 2.

Naphthalene (mean: 25 pg.m⁻³ min-max: 10-98 pg.m⁻³, n=9) is the most volatile (11 Pa at 298K) of the targeted PAHs making it difficult to sample using the described methodology. Because of this the sum of PAHs is reported without naphthalene as $\Sigma_{15}PAH$ which is common in similar studies (Harner et al., 2013). Naphthalene is excluded from the synthesizing figures and the discussion unless explicitly mentioned. Average concentrations of the $\Sigma_{15}PAH$ for the gas and particulate phase of 41 ± 40 and 1.5 ± 2.7 pg m⁻³, and 26 ± 11 and 11 ± 9.4 pg m⁻³ for the $\Sigma_{13}OPAHS$ in the gas and particulate phase respectively are found. The full PAH and oxy-PAH dataset is made available in S.I. 13 to S.I. 16.

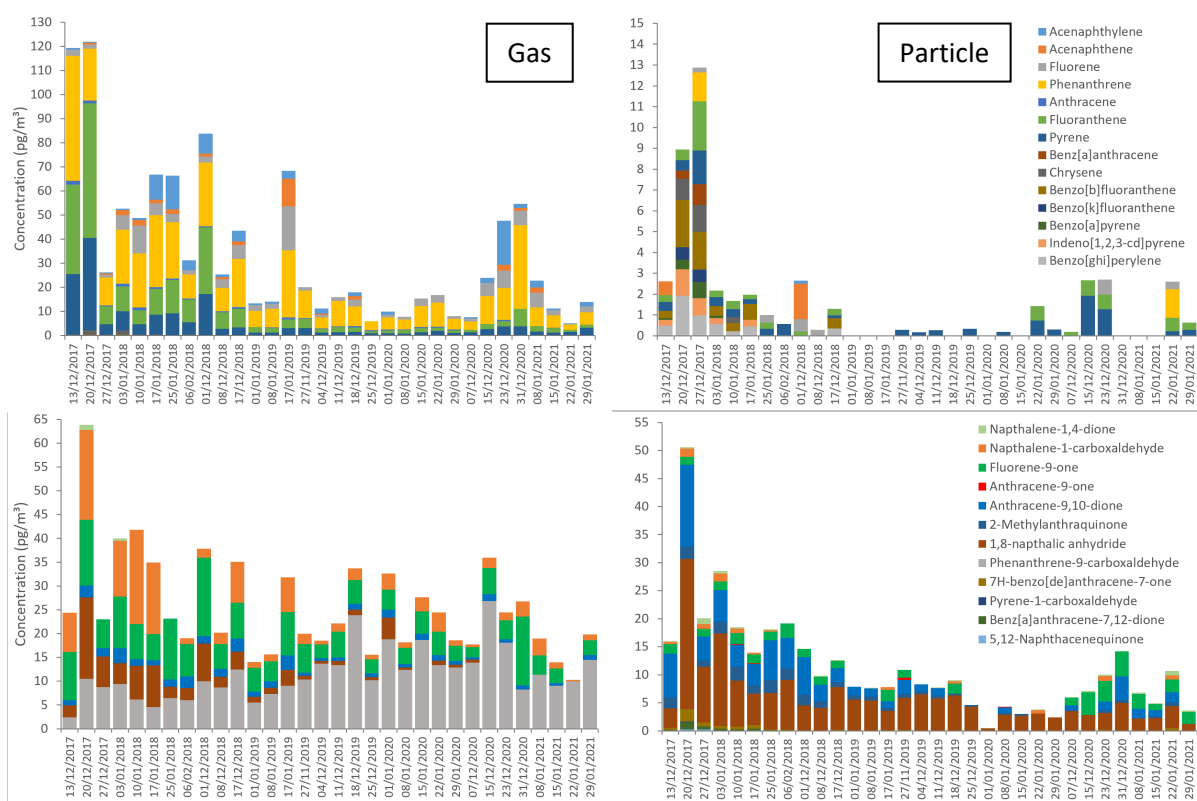


Figure 2: Stacked concentrations of the 14 PAHs and 12 OPAHs measured from 2017 to 2021, split up according to the compound group and the phase they were measured in. Concentration reported as pg compound per normalized (1013 hPa and 25 °C) m³ of air. Note the different ordinate scales.

Phenanthrene, fluoranthene and pyrene were found to be the most abundant PAHs contributing 44, 17 and 13 % respectively to the $\Sigma_{15}\text{PAH}$ in the combined sample. This is a very similar to (Cao et al., 2018; Zhang et al., 2021) and (Na et al., 2020) who reported phenanthrene at the Antarctic peninsula contributing to 40, 43 and 55 % of the total PAH concentration and other authors indicating phenanthrene was the predominant compound in Antarctica (Cabrerizo et al., 2014; Caricchia et al., 1995; Piazza et al., 2013). For the oxy-PAHs, in the gas phase, phenanthrene-9-carboxaldehyde is the most dominant compound (50%) followed by fluorene-9-one (25%) while in the particle phase 1,8-naphthalic anhydride is the largest contributor to the total oxy-PAH concentration measured (55%).

The highest concentrations are observed for both PAHs and oxy-PAHs during the 2017-2018 summer season. In general, 3 ring compounds are the largest contributor to the total PAH and oxy-PAH concentration with the 2017-18 summer being a notable exception when, compared to 3-ring PAHs (35 pg m⁻³), an almost equal contribution of 4-ring PAHs is measured (34 pg m⁻³). That specific summer is also the only time during the 4-year campaign when a detectable amount (1pg m⁻³) of 6-ring PAHs was measured. A possible explanation for the found variance is the heightened volcanic activity in the southern hemisphere in the period before and during the measurement which is further discussed in Section 3.6. The interannual differences between the 2018-19, 2019-20 and 2022-21 campaign are more subtle with maybe the most striking difference being the oxy-PAH fraction ($\Sigma_{12}\text{oxyPAH}/\Sigma_{15}\text{PAH}$) which is 0.8 for 2018-19 and rises to 2.0 for the 2019-20 summer season and then relaxes again to 1.1 indicating both groups are present in about an equal concentration.

In Figure 3A the average total PAH and oxy-PAH concentration per sampling season is given per number of rings. For PAHs, 3-ring compounds dominate the gas phase (73% of the total mass, average) while in the particle phase they are less present (16%). This is to be expected as the gas/particle

partitioning of a compound is related with the vapor pressure and thus the number of rings in the structure (Ravindra et al., 2008). In Figure 3B the partitioning of PAHs in relation to the number of rings is clear. A dominance of 4, 5 and 6-ring compounds in the particle phase is observed. This is in line with (Zhang et al., 2021) who found, during a cruise from China to Antarctica, five and six ring PAHs only contributed for 0.59 and 0.21% to the total gaseous PAH concentration. For oxy-PAHs the partitioning between both phases is less pronounced.

Despite PAHs showing a longer atmospheric lifetime when associated to a particle, a factor 32 (median) higher concentration is found in the gas phase compared to the particle phase. A more equal distribution is found for the oxy-PAHs with a factor 2.5 (median) higher concentrations found in the gas phase. This observation is very interesting. The particle number at PEA is very low and dominated by smaller particles (Herenz et al., 2019). The fact that only a minor fraction of the total PAH mass is found on the QFF is likely attributed to significant deposition (wet or dry) of particles during the transport from the source. This hypothesis implies that the oxy-PAHs are either condensing into aerosols after their formation by the reaction of PAHs with $\cdot\text{OH}$ or that they, because of their increased polarity, show a higher affinity for the sampled particles. This observation is an interesting subject to further explore in the future as cloud formation and microphysics are interlinked with the type of particle and associated compounds.

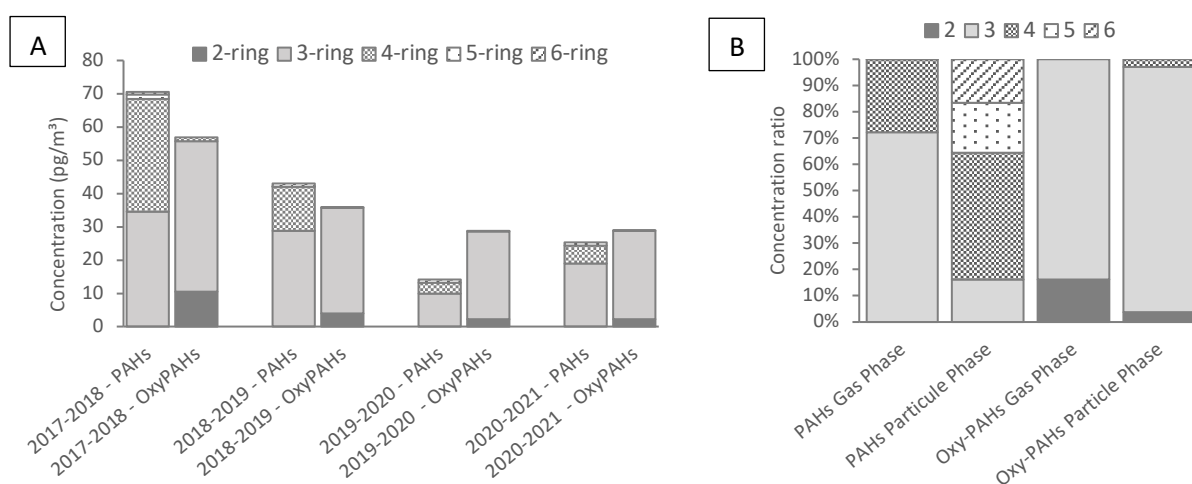


Figure 3A: The contribution to the total PAH and oxy-PAH concentration of the total (gas + particle) sample in pg m^{-3} split up per number of rings in the structure on the left. 3B: The relative contribution per number of rings to the total PAH and oxy-PAH concentration of the gas and particulate phase.

Oxy-PAHs are found in the concentration levels of the same order of magnitude as PAHs which is in accordance to what (Albinet et al., 2008) found in the French alps. A significant (ANOVA, 99% C.I.) linear relationship is found for the $\Sigma_{15}\text{PAH}$ and $\Sigma_{12}\text{oxy-PAH}$ concentrations of the total sample (Figure 5). This indicates a common source for both compound groups and that photodegradation of PAHs is indeed an important process. This is supported by the fact that compounds which show a higher photochemical reactivity such as anthracene and benzo[a]anthracene are found in much lower levels, or not at all, when compared to their corresponding isomers phenanthrene and chrysene.

Intercorrelation for all compounds was evaluated. Pyrene and fluoranthene, both 4 ring compounds, displayed a significant linear relationship for the complete sampling campaign (Figure 4). This observation suggests a common source and atmospheric transport pathway for both compounds. Remarkably the 2nd order reaction rate of pyrene with $\cdot\text{OH}$ ($5.0 \times 10^{-11} \text{ cm}^3 \text{ molec}^{-1} \text{ s}^{-1}$) is 5 times higher compared to fluoranthene ($1.1 \times 10^{-11} \text{ cm}^3 \text{ molec}^{-1} \text{ s}^{-1}$) resulting in an atmospheric lifetime of 5.5h and

25h respectively using a $[\text{OH}]$ concentration of $10^6 \text{ molecules cm}^{-3}$ (Atkinson and Arey, 1994; Brubaker and Hites, 1998; Keyte et al., 2013). Thus, a steeper slope is expected if transport occurs via the gas phase only. As the reaction rates of the heterogenous reaction of OH with particle bound pyrene (1.6 to $320 \times 10^{-14} \text{ cm}^3 \text{ molec}^{-1} \text{ s}^{-1}$) and fluoranthene (1.4 to $320 \times 10^{-14} \text{ cm}^3 \text{ molec}^{-1} \text{ s}^{-1}$) (Keyte et al., 2013) are much smaller and approximately equal, transport via the particle phase offers a better explanation for the observed trend. This supports atmospheric transport of PAHs is driven by the transport of particles.

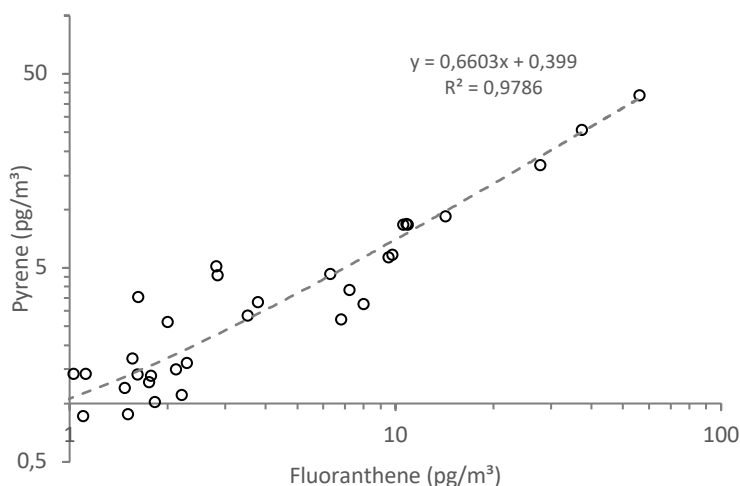


Figure 4: Correlation between pyrene and fluoranthene concentrations (sum of gas and particle phase). Note the logarithmic scale axis.

With most of the research on PAHs in Antarctica done on the Antarctic Peninsula it is hard to compare with the obtained data as concentrations reported in that area are at least a factor 10 higher. (Na et al., 2020) reported concentrations of 15 EPA PAHs (gas: mean 6489 pg m^{-3} , min-max: $357\text{--}58567 \text{ pg m}^{-3}$, particle: mean 645 pg m^{-3} , min-max: $17.1\text{--}7215 \text{ pg m}^{-3}$) from a 7-year monitoring campaign during the summers from 2013 to 2019. (Cabrerizo et al., 2014) and (Cao et al., 2018) report similar concentrations from a cruise in the seas surrounding the peninsula during the austral summers of 2005, 2008 and 2009 and the summer of 2014. The concentration levels reported in this study agree better with those reported by (Caricchia et al., 1995) (15 and 700 pg m^{-3}) and (Piazza et al., 2013) measured at Terra Nova Bay during the summers of 1991, 1992 and 2009-2010. Of the latter, only (Piazza et al., 2013) used a PUF and QFF filter to separately collect PAHs in the gaseous and particle phase, and reported concentrations between 21 and 328 pg m^{-3} for the sum of $\sum_{15}\text{PAH}$ in both phases.

This large variability in atmospheric PAH concentrations is explained by high levels of anthropogenic activity on the peninsula. According to (COMNAP, 2017) 39 facilities are active on the peninsula and the surrounding islands compared to 5 in Victoria Land, the region encompassing Terra Nova Bay. Furthermore, tourism to Antarctica is largely focused on this region (IAATO, 2020), both factors inevitably have an effect on the PAH concentration in the environment (Vodopivec et al., 2021). Previous research reported the source of PAHs measured at the Peninsula is human activities rather than LRAT (Cao et al., 2018; Na et al., 2020) while (Cabrerizo et al., 2014) also reported the revolatilization from soil and snow as a secondary source.

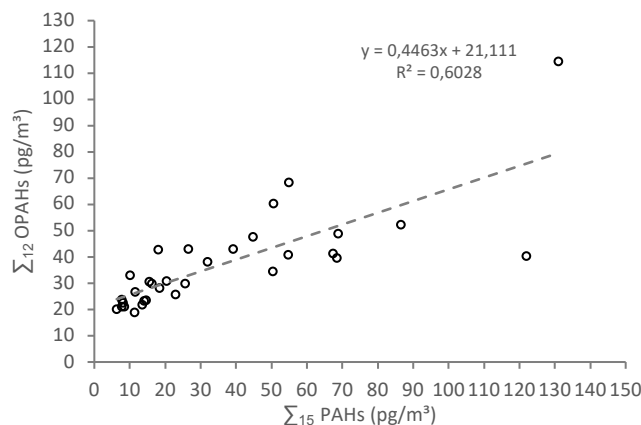


Figure 5: Relation between $\Sigma_{15}\text{PAH}$ and $\Sigma_{12}\text{Oxy-PAH}$ concentration for the combined sample expressed as a linear relationship.

Because of the low gas and particle phase concentrations of PAHs and the sheer distance from anthropogenic sources it is concluded the atmospheric concentrations reported in this study are solely influenced by LRAT and are not directly influenced by anthropogenic activities. Contrary to (Cabrerizo et al., 2014), no significant dependence of the gaseous PAH concentration with temperature was found and thus revolatilization from the surrounding surface was not considered an important driver for the measured PAHs.

3.3 Gas-particle partitioning

The gas-particle partitioning coefficient ($K_{p,i}$) was calculated with equation (2) in accordance with (Fernández et al., 2002) where $C_{g,i}$ and $C_{p,i}$ are the measured concentrations (pg m^{-3}) of compound i in the gas phase and particle phase respectively and C_{TSP} is the concentration of total suspended particles ($\mu\text{g m}^{-3}$).

$$K_{p,i} = \frac{C_{p,i}}{C_{g,i} \cdot C_{\text{TSP}}}$$

(2)

The C_{TSP} for each sample is calculated as explained in Section 2.7 **Erreur ! Source du renvoi introuvable..** Although some care should be taken interpreting the TSP data as an error of $\pm 0.5 \mu\text{g m}^{-3}$ is to be expected and rocky outcrops close to the sample site might have an influence. However, it was noted that the variance of K_p decreased by including the TSP data recorded by the TEOM-FDMS compared to substituting C_{TSP} with a constant value. A histogram of the TSP concentrations measured during the HVS sample periods is given in S.I. 18 and shows a normal distribution around $3.1 \mu\text{g m}^{-3}$ which is similar to other studies (Budhavant et al., 2015; Lugar, 1994). For the 2017-18 summer no TSP data are available, and the average of the other sample periods is used for the calculation of K_p . Only six compounds which occurred in both the gas and particle phase in the same sample in at least 10 instances are considered for calculating the partitioning coefficient. Because of the remote nature of the sampling site, gas/particle phase concentrations can be considered in equilibrium. Within the limited temperature range during sampling (261-267 K mean: 264 K) no significant relation between temperature and the gas phase PAH concentration is found. Indicating that the PAH concentration is controlled by LRAT (Wania et al., 1998). Results for K_p are shown as boxplots containing data of the 4 campaigns per compound in Figure 6.

For the 2 PAHs for which $\log(K_p)$ was calculated, fluoranthene and pyrene, a median value of -1.6 and -1.4 is found. Very few studies report K_p for similar remote and cold environments. (Fernández et al.,

2002) presents K_p for selected PAHs in high mountain regions in Europe and found a K_p of -2.2 (at 274 K) and -1.7 (at 273K) for fluoranthene in the Catalan Pyrenees and the Tyrolean Alps respectively and -2.1 and -1.3 for pyrene at the same locations. The difference between the coefficients reported by (Fernández et al., 2002) and the ones reported in this study might be solely explained by the 10 K temperature difference. (van Drooge et al., 2010) found a $\log(K_p)$ of -1.5 for fluoranthene and -0.9 for pyrene at 264 K albeit the measurement site in the High Tatras is reported by the authors to be more influenced by air masses from industrial and urbanized areas. During a cruise in the southern ocean (Zhang et al., 2021) measured a median $\log(K_p)$ of -1.8 and -2.1 for fluoranthene and pyrene for air masses originating from Antarctica, but again measured at higher temperatures.

K_p was also calculated for 4 oxy-PAHs, median values of 0.1, -0.1, -1.0 and -1.3 were obtained for 1,8-naphthalic anhydride, anthracene-9,10-dione, fluorene-9-one and naphthalene-1-carboxaldehyde respectively. For the oxy-PAHs number of relevant studies is even more limited. In Svalbard, (Drotikova et al., 2020) determined PAHs and oxy-PAHs in the gas and particulate phase but didn't report the partitioning coefficient for the measured compounds. Instead, they reported between 26 and 42 % of fluorene-9-one and between 45 and 38 % of anthracene-9,10-dione occurs in the particle phase. Similarly, during the measurements reported in this study, on average 68% of anthracene-9,10-dione and 24% of fluorene-9-one exists in particle gas phase. (Albinet et al., 2008) measured oxy-PAHs in two alpine valleys in France. The report doesn't specify partition coefficients per compound but from the data in the SI an average $\log(K_p)$ of -2.1 and -1.2 for naphthalene-1-carboxaldehyde and fluorene-9-one is calculated for an average temperature of 269.5 K. Contrary to (Drotikova et al., 2020) and this study (Albinet et al., 2008) reports anthracene-9,10-dione occurs almost exclusively in the particle phase. For 1,8-naphthalic anhydride no published data on its partitioning in cold and remote environments was found. It is recommended to continue and expand measurements of PAHs and atmospheric reaction products. Longer data series over a broader temperature range will aid in determining K_p of the different compounds experimentally for cold conditions and allow to observe changes in partitioning considering a changing climate.

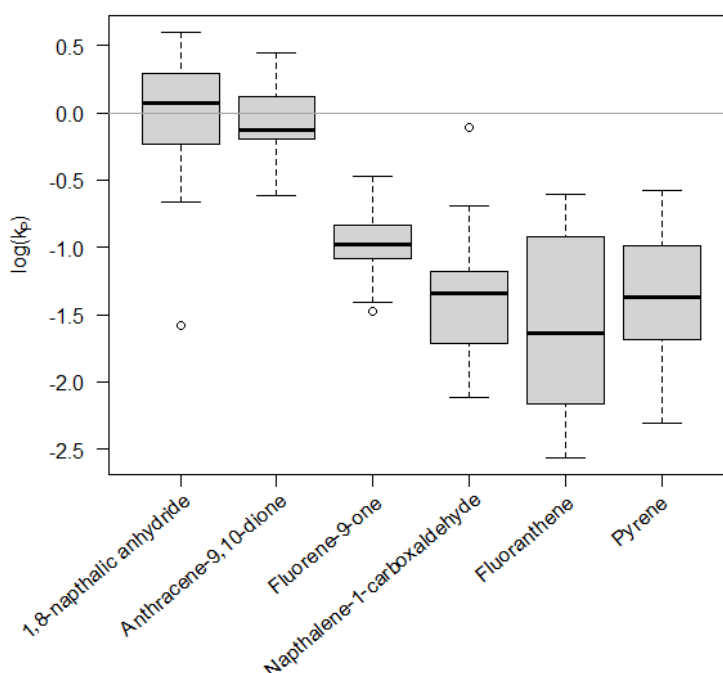


Figure 6: The logarithm of the gas particle partitioning coefficient for the 6 compounds which were frequently (i.e. more than 10 instances) quantified.

3.4 Molecular diagnostic ratios

The usage of molecular diagnostic ratios (MDRs) for PAHs has been subject of discussion and is reported as severely influenced by seasonality and not suitable for source appointment. The general consensus states MDRs should be used with caution (Katsoyiannis et al., 2011; Tobiszewski and Namieśnik, 2012). Especially since this study deals with aged air masses, severely skewing the ratios, a thorough description of all frequently used MDRs, which are often based on measurements close to the emission source, might lead to wrong conclusions. Despite this, it is worth discussing the fluorene (FL)/pyrene (PYR) ratio of the total sample (particle + gas phase) which shows high variability (0.04 – 6.5, median: 1.1) as shown in Figure 7. It is difficult to determine what contributes to the variation found in the data but (Kozak et al., 2017) found a higher FL/PYR ratio in water samples in Svalbard during periods with episodes of volcanic eruptions. The influence of volcanic activity on the measurements is further explored in section 3.6.

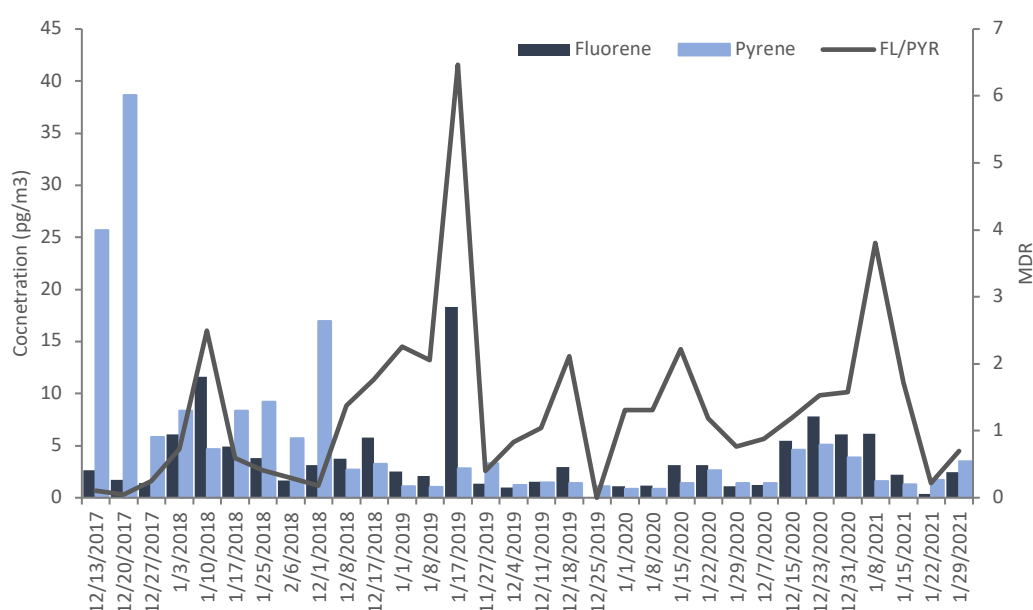


Figure 7: Concentration (pg m^{-3}) and molecular diagnostic ratio (MDR) of fluorene/pyrene for the total sample.

3.5 PMF source-receptor modeling

The best fit of the data to the model was obtained using a 6-factor PMF model. The fingerprint for each factor is shown in S.I. 19. The six resulting factors suggest six different sources/influxes which is opposed to the assumed 4 theoretical influxes (Continental, Southern South America, Southern Africa, Oceania) (Mangold et al., 2021). Though it is impossible with the measured and modeled information to exactly determine the exact source corresponding to each factor, some trends are discussed. Figure 8 shows the relative contribution of each factor to each individual sample.

Factor 1 is mainly loaded with phenanthrene, fluoranthene and pyrene. As shown in Figure 4 a linear relation between the latter two is found indicating a common source. Phenanthrene doesn't correlate with FLA or PYR which points to other sources contributing to the measured PHE concentration. This hypothesis is confirmed as phenanthrene is a major contributor to factor 2 and 3 as well. For factor 2, 3 and 4 such a clear observation is absent. As significant amounts of oxy-PAHs are reported by these factors all three appear to represent significantly aged air masses. The profile of factor 4 contains high amounts of 1,8-naphthalic anhydride and 1-naphthalenecarboxaldehyde which are both reported as formed from acenaphthene and acenaphthylene by the reaction with $\cdot\text{OH}$ and O_3 (Srivastava et al.,

2022). In both factor 2 and 3 the oxy-PAHs of the corresponding parent PAHs are found. E.g., phenanthrene-9-carboxaldehyde and phenanthrene. Factor 5 is defined by mainly LMW 3-ring PAHs which occur in the gas phase, contrary to factor 6 which is heavily loaded by compounds having a significant affinity with the particle phase. This also corresponds with the information already shown in Figure 2. The samples started on 20/12 and 27/12/2017 clearly show a peak in particle bound PAHs as factor 6 contributes more to the sample.

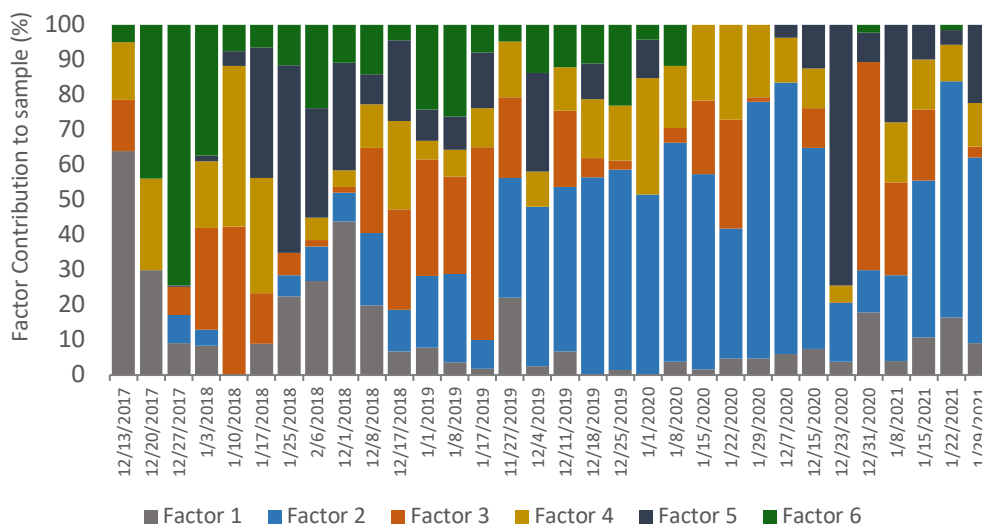


Figure 8: Relative factor contribution per PMF considering a 6-factor model for all samples collected during the austral summers of 2017 to 2021 at the Princess Elisabeth station.

3.6 Dispersion modeling and volcanic influence

Backward dispersion analysis was performed to determine which source regions can be associated with the observations made during the measurement campaign. Special interest goes to volcanic eruptions as these evoke a strong PAH transient at large altitude and are very well reported. The amount and type of PAHs emitted on the other hand is not well studied. (Kozak et al., 2017) studied PAHs in soils in Spitsbergen which are influenced by volcanic activity in Iceland and (Guiñez et al., 2020) analyzed nitro and oxy-PAHs in volcanic ash. However, the direct detection of atmospheric PAHs in an air mass influenced by volcanic activity has never been reported before.

Figure 9 shows all eruptions, with a volcanic explosivity index (VEI) larger or equal than 2 which occurred from September 2017 to the end of the measurement campaign from volcanoes between 90° S and 15° N (Smithsonian Institution, 2023), combined with the measured PAH concentrations.

During the measurement campaign, one eruption with a VEI of 4 is recorded on the 12/01/2020 (Taal Volcano, the Philippines, 14°0'N 120°59'E). While the last sample stopped on the 5th of February no signal for this eruption was recorded, indicating transport to East-Antarctica either didn't happen as the volcano lies north of the equator or that it took longer than 24 days to reach the measurement site. Nevertheless, volcanic signals were recorded for other eruptions, mainly with a VEI of 3, which occurred during the austral summers of 2017 to 2021.

One prime example is the December 2018 eruption of the Anak Krakatau (Indonesia, 6°06' S 105°25' E) from 22/12/2018 to 06/01/2019. A remarkable rise in the total PAH concentration is recorded for the sample taken from 17/01/2019 to 24/01/2019 reaching 210 pg m⁻³ making it the 2nd highest concentration measured overall. This corresponds to a transport time between 11 and 33 days. The backwards dispersion model for this sample period shows the airmass measured is indeed influenced

by the eruption (Figure 10). Running a forward dispersion model using the eruption data as reported in (Goodier and Paris, 2019) and a 15 km plume height, the air mass arrives 21/01/2019 at 6.00 UTC at the measurement site, confirming the rise in PAH concentration is indeed associated with the eruption of the Anak Krakatau. This observation proves the hypothesis that PAHs can be transported over long distances to remote areas via atmospheric transport under certain conditions, as well as the significant impact of natural sources.

Considering the time between eruption and measurement, the eruptions of the Tinakula (Solomon Islands, 10°23' S 165°48' E) on 21/10/2017 and of the Agung (Indonesia, 8°20' S 115°30' E) on 27/11/2017 are proposed as contributors to the elevated PAH levels measured during the first half of the 2017-2018 measurement campaign. As far as we know this is the first report describing a direct observation of the influence of volcanic eruptions on PAH levels in the atmosphere. Proving the potential for LRAT and prolonged atmospheric lifetimes of PAHs.

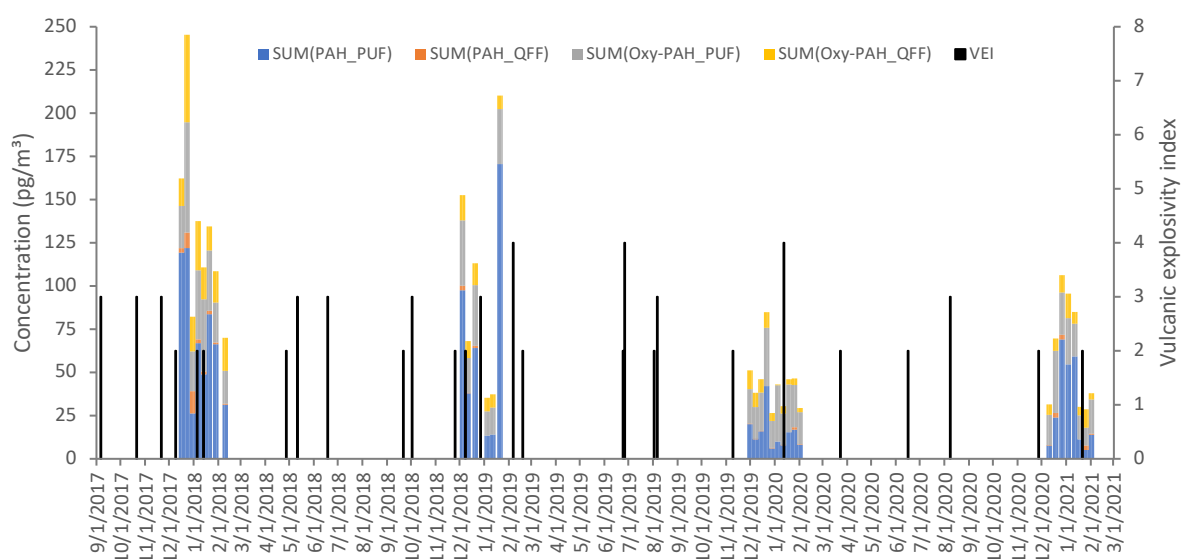


Figure 9: Concentration of PAHs and oxy-PAHs in the gas and particle phase measured at the Princess Elisabeth Station combined with volcanic eruption data (VEI ≥ 2 and between 90°S and 15°N)

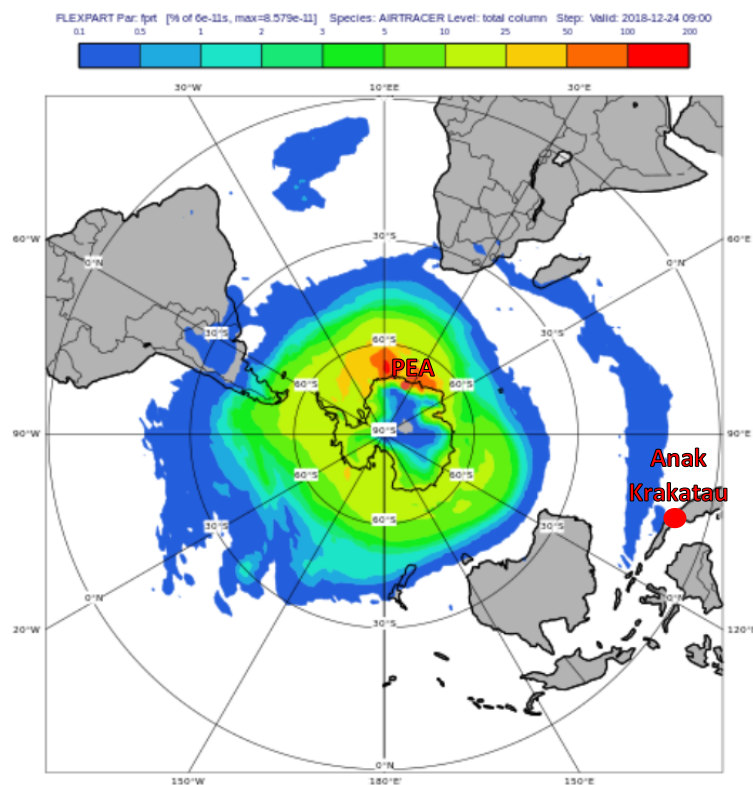


Figure 10: Output showing the relative residence time for the thirty day backward dispersion analysis with the Princess Elisabeth Station as the receptor point for the sample period between 17/01/2019 and 24/01/2019. Residence time is summed from 5000 to 10000 m altitude. No wet or dry deposition is considered

4 Acknowledgements

We acknowledge the financial support of the Belgian Science Policy office (BELSPO) in the framework of the CHASE (BR/175/A2/CHASE) project. The financial support by the special research fund (BOF) in the form of SG for Christophe Walgraeve and in the framework of the Flemish investment support for heavy research equipment and FWO-funding (1.5.062.09.N.00) for analytical equipment support. We would like to express our gratitude to the International Polar Foundation (IPF), to Nighat "Gigi" Johnson-Amin, Alain Hubert, Henri Robert, the support engineers Benoît Verdin and Johnny Gaelens, and all personnel deployed at, and in support of the Princess Elisabeth Station.

5 References

- Albinet, A., Leoz-Garziandia, E., Budzinski, H., Villenave, E., Jaffrezo, J.L., 2008. Nitrated and oxygenated derivatives of polycyclic aromatic hydrocarbons in the ambient air of two French alpine valleys. Part 1: Concentrations, sources and gas/particle partitioning. *Atmos. Environ.* 42, 43–54. <https://doi.org/10.1016/j.atmosenv.2007.10.009>
- Andersson, J.T., Achten, C., 2015. Time to Say Goodbye to the 16 EPA PAHs? Toward an Up-to-Date Use of PACs for Environmental Purposes. *Polycycl. Aromat. Compd.* 35, 330–354. <https://doi.org/10.1080/10406638.2014.991042>
- Atkinson, R., Arey, J., 1994. Atmospheric Chemistry of Gas-Phase Polycyclic Aromatic Hydrocarbons: Formation of Atmospheric Mutagens. *Environ. Health Perspect.* 102, 117. <https://doi.org/10.2307/3431940>
- Bidleman, T.F., 1988. Atmospheric processes. *Environ. Sci. Technol.* 22, 361–367. <https://doi.org/10.1021/es00169a002>
- Brubaker, W.W., Hites, R.A., 1998. OH Reaction Kinetics of Polycyclic Aromatic Hydrocarbons and Polychlorinated Dibenzo-p-dioxins and Dibenzofurans. *J. Phys. Chem. A* 102, 915–921. <https://doi.org/10.1021/jp9721199>
- Budhavant, K., Safai, P.D., Rao, P.S.P., 2015. Sources and elemental composition of summer aerosols in the Larsemann Hills (Antarctica). *Environ. Sci. Pollut. Res.* 22, 2041–2050. <https://doi.org/10.1007/s11356-014-3452-0>
- Cabrerizo, A., Galbán-Malagón, C., Del Vento, S., Dachs, J., 2014. Sources and fate of polycyclic aromatic hydrocarbons in the Antarctic and Southern Ocean atmosphere. *Global Biogeochem. Cycles* 28, 1424–1436. <https://doi.org/10.1002/2014GB004910>
- Cao, S., Na, G., Li, R., Ge, L., Gao, H., Jin, S., Hou, C., Gao, Y., Zhang, Z., 2018. Fate and deposition of polycyclic aromatic hydrocarbons in the Bransfield Strait, Antarctica. *Mar. Pollut. Bull.* 137, 533–541. <https://doi.org/10.1016/j.marpolbul.2018.10.045>
- Caricchia, A.M., Chiavarini, S., Cremisini, C., Morabito, R., Perini, A., Pezza, M., 1995. Determination of PAH in atmospheric particulates in the area of the Italian base in Antarctica: Report on monitoring activities during the last three scientific expeditions. *Environ. Pollut.* 87, 345–356. [https://doi.org/10.1016/0269-7491\(94\)P4166-L](https://doi.org/10.1016/0269-7491(94)P4166-L)
- Clergé, A., Le Goff, J., Lopez, C., Ledauphin, J., Delépée, R., 2019. Oxy-PAHs: occurrence in the environment and potential genotoxic/mutagenic risk assessment for human health. *Crit. Rev. Toxicol.* 49, 302–328. <https://doi.org/10.1080/10408444.2019.1605333>
- COMNAP, 2017. Antarctic Station Catalogue.
- Drotikova, T., Ali, A.M., Karine Halse, A., Reinardy, H.C., Kallenborn, R., 2020. Polycyclic aromatic hydrocarbons (PAHs) and oxy- And nitro-PAHs in ambient air of the Arctic town Longyearbyen, Svalbard. *Atmos. Chem. Phys.* 20, 9997–10014. <https://doi.org/10.5194/acp-20-9997-2020>
- Fernández, P., Grimalt, J.O., Vilanova, R.M., 2002. Atmospheric gas-particle partitioning of polycyclic aromatic hydrocarbons in high mountain regions of Europe. *Environ. Sci. Technol.* 36, 1162–1168. <https://doi.org/10.1021/es010190t>
- Friedman, C.L., Selin, N.E., 2012. Long-range atmospheric transport of polycyclic aromatic hydrocarbons: A global 3-D model analysis including evaluation of arctic sources. *Environ. Sci. Technol.* 46, 9501–9510. <https://doi.org/10.1021/es301904d>
- Goodier, M., Paris, R., 2019. SO₂ and tephra emissions during the December 22, 2018 Anak Krakatau flank-collapse eruption. *Volcanica* 2, 91–103. <https://doi.org/10.30909/vol.02.02.91103>
- Gorodetskaya, I. V., Kneifel, S., Maahn, M., Thiery, W., Schween, J.H., Mangold, A., Crewell, S., Van Lipzig, N.P.M., 2015. Cloud and precipitation properties from ground-based remote-sensing instruments in East Antarctica. *Cryosphere* 9, 285–304. <https://doi.org/10.5194/tc-9-285-2015>
- Gorodetskaya, I. V., Van Lipzig, N.P.M., Van Den Broeke, M.R., Mangold, A., Boot, W., Reijmer, C.H., 2013. Meteorological regimes and accumulation patterns at Utsteinen, Dronning Maud Land, East Antarctica: Analysis of two contrasting years. *J. Geophys. Res. Atmos.* 118, 1700–1715. <https://doi.org/10.1002/jgrd.50177>
- Guiñez, M., Escudero, L., Mandelli, A., Martinez, L.D., Cerutti, S., 2020. Volcanic ashes as a source for nitrated and oxygenated polycyclic aromatic hydrocarbon pollution. *Environ. Sci. Pollut. Res.* 27, 16972–16982. <https://doi.org/10.1007/s11356-020-08130-7>
- Harner, T., Su, K., Genualdi, S., Karpowicz, J., Ahrens, L., Mihele, C., Schuster, J., Charland, J.-P., Narayan, J., 2013. Calibration and application of PUF disk passive air samplers for tracking polycyclic aromatic compounds (PACs). *Atmos. Environ.* 75, 123–128. <https://doi.org/10.1016/j.atmosenv.2013.04.012>
- He, J., Balasubramanian, R., 2009. Determination of atmospheric polycyclic aromatic hydrocarbons using accelerated solvent

547 extraction. *Anal. Lett.* 42, 1603–1619. <https://doi.org/10.1080/00032710902993886>

548 Herenz, P., Wex, H., Mangold, A., Laffineur, Q., Gorodetskaya, I. V., Fleming, Z.L., Panagi, M., Stratmann, F., 2019. CCN
549 measurements at the Princess Elisabeth Antarctica research station during three austral summers. *Atmos. Chem. Phys.*
550 19, 275–294. <https://doi.org/10.5194/acp-19-275-2019>

551 IAATO, 2020. IAATO Antarctic visitor figures 2019-2020.

552 Katsoyiannis, A., Sweetman, A.J., Jones, K.C., 2011. PAH molecular diagnostic ratios applied to atmospheric sources: A critical
553 evaluation using two decades of source inventory and air concentration data from the UK. *Environ. Sci. Technol.* 45,
554 8897–8906. <https://doi.org/10.1021/es202277u>

555 Keyte, I.J., Harrison, R.M., Lammel, G., 2013. Chemical reactivity and long-range transport potential of polycyclic aromatic
556 hydrocarbons-a review. *Chem. Soc. Rev.* 42, 9333–9391. <https://doi.org/10.1039/c3cs60147a>

557 Kozak, K., Ruman, M., Kosek, K., Karasiński, G., Stachnik, Ł., Polkowska, Z., 2017. Impact of volcanic eruptions on the
558 occurrence of PAHs compounds in the aquatic ecosystem of the southern part of West Spitsbergen (Hornsund Fjord,
559 Svalbard). *Water (Switzerland)* 9. <https://doi.org/10.3390/w9010042>

560 Kukučka, P., Lammel, G., Dvorská, A., Klánová, J., Möller, A., Fries, E., 2010. Contamination of Antarctic snow by polycyclic
561 aromatic hydrocarbons dominated by combustion sources in the polar region. *Environ. Chem.* 7, 504.
562 <https://doi.org/10.1071/EN10066>

563 Li, R., Hua, P., Krebs, P., 2022. Global Trends and Drivers in Consumption- and Income-Based Emissions of Polycyclic Aromatic
564 Hydrocarbons. *Environ. Sci. Technol.* 56, 131–144. <https://doi.org/10.1021/acs.est.1c04685>

565 Lohmann, R., Gioia, R., Jones, K.C., Nizzetto, L., Temme, C., Xie, Z., Schulz-Bull, D., Hand, I., Morgan, E., Jantunen, L., 2009.
566 Organochlorine pesticides and PAHs in the surface water and atmosphere of the North Atlantic and Arctic Ocean.
567 *Environ. Sci. Technol.* 43, 5633–5639. <https://doi.org/10.1021/es901229k>

568 Lugar, R.M., 1994. FY 1994 Ambient Air Monitoring Report for McMurdo Station, Antarctica 1–71.

569 Lundstedt, S., White, P.A., Lemieux, C.L., Lynes, K.D., Lambert, I.B., Öberg, L., Haglund, P., Tysklind, M., 2007. Sources, fate,
570 and toxic hazards of oxygenated Polycyclic Aromatic Hydrocarbons (PAHs) at PAH-contaminated sites. *Ambio* 36, 475–
571 485. [https://doi.org/10.1579/0044-7447\(2007\)36\[475:SFATHO\]2.0.CO;2](https://doi.org/10.1579/0044-7447(2007)36[475:SFATHO]2.0.CO;2)

572 Mangold, A., De Causmaecker, K., Decloo, A., Laffineur, Q., Van Overmeiren, P., Walgraeve, C., Demeestere, K., Van
573 Langenhove, H., Gili, S., Vanderstraeten, A., Mattioli, N., 2021. Climatology of air mass origin for Princess Elisabeth
574 Antarctica station: clustering and analysis for atmospheric particle properties and semi-Volatile Organic Compounds,
575 in: *European Aerosol Conference, Abstracts*. Birmingham, UK.

576 Na, G., Gao, Y., Li, R., Gao, H., Hou, C., Ye, J., Jin, S., Zhang, Z., 2020. Occurrence and sources of polycyclic aromatic
577 hydrocarbons in atmosphere and soil from 2013 to 2019 in the Fildes Peninsula, Antarctica. *Mar. Pollut. Bull.* 156,
578 111173. <https://doi.org/10.1016/j.marpolbul.2020.111173>

579 Paatero, P., Tapper, U., 1994. Positive matrix factorization: A non-negative factor model with optimal utilization of error
580 estimates of data values. *Environmetrics* 5, 111–126. <https://doi.org/10.1002/env.3170050203>

581 Pattyn, F., Matsuoka, K., Berte, J., 2009. Glacio-meteorological conditions in the vicinity of the Belgian Princess Elisabeth
582 Station, Antarctica. *Antarct. Sci.* 22, 79–85. <https://doi.org/10.1017/S0954102009990344>

583 Piazza, R., Gambaro, A., Argiriadis, E., Vecchiato, M., Zambon, S., Cescon, P., Barbante, C., 2013. Development of a method
584 for simultaneous analysis of PCDDs, PCDFs, PCBs, PBDEs, PCNs and PAHs in Antarctic air. *Anal Bioanal Chem* 405, 917–
585 932. <https://doi.org/10.1007/s00216-012-6464-y>

586 Ravindra, K., Sokhi, R., Van Grieken, R., 2008. Atmospheric polycyclic aromatic hydrocarbons: Source attribution, emission
587 factors and regulation. *Atmos. Environ.* 42, 2895–2921. <https://doi.org/10.1016/j.atmosenv.2007.12.010>

588 Smithsonian Institution, 2023. Global Volcanism Program, 2023. [Database] *Volcanoes of the World* (v. 5.0.3; 1 Mar 2023).
589 Compiled by Venzke, E. [WWW Document]. <https://doi.org/https://doi.org/10.5479/si.GVP.VOTW5-2022.5.0>

590 Souverijns, N., Gossart, A., Gorodetskaya, I. V., Lhermitte, S., Mangold, A., Laffineur, Q., Delcloo, A., Van Lipzig, N.P.M., 2018.
591 How does the ice sheet surface mass balance relate to snowfall? Insights from a ground-based precipitation radar in
592 East Antarctica. *Cryosphere* 12, 1987–2003. <https://doi.org/10.5194/tc-12-1987-2018>

593 Srivastava, D., Vu, T. V., Tong, S., Shi, Z., Harrison, R.M., 2022. Formation of secondary organic aerosols from anthropogenic
594 precursors in laboratory studies. *npj Clim. Atmos. Sci.* 5. <https://doi.org/10.1038/s41612-022-00238-6>

595 Stohl, A., Forster, C., Frank, A., Seibert, P., Wotawa, G., 2005. Technical note: The Lagrangian particle dispersion model
596 FLEXPART version 6.2. *Atmos. Chem. Phys.* 5, 2461–2474. <https://doi.org/10.5194/acp-5-2461-2005>

597 Tobiszewski, M., Namieśnik, J., 2012. PAH diagnostic ratios for the identification of pollution emission sources. *Environ.*
598 *Pollut.* 162, 110–119. <https://doi.org/10.1016/j.envpol.2011.10.025>

599 U.S. Environmental Protection Agency, 2014. EPA Positive Matrix Factorization (PMF) 5.0 Fundamentals and User Guide.

600 UNECE, 1998. The 1998 Aarhus Protocol on Persistent Organic Pollutants (POPs).

601 van Drooge, B.L., Fernández, P., Grimalt, J.O., Stuchlík, E., García, C.J.T., Cuevas, E., 2010. Atmospheric polycyclic aromatic
602 hydrocarbons in remote European and Atlantic sites located above the boundary mixing layer. *Environ. Sci. Pollut. Res.*
603 17, 1207–1216. <https://doi.org/10.1007/s11356-010-0296-0>

604 Vodopivec, C., Curtosi, A., Pelletier, E., Saint-Louis, R., Spairani, L.U., Hernández, E.A., Zakrajsek, A., Genez, A., Mac Cormack,
605 W.P., 2021. Low levels of PAHs and organotin compounds in surface sediment samples from a broad marine area of
606 25 de Mayo (King George) Island, South Shetland Islands. *Sci. Total Environ.* 785.
607 <https://doi.org/10.1016/j.scitotenv.2021.147206>

608 Walgraeve, C., Chantara, S., Sopajaree, K., De Wispelaere, P., Demeestere, K., Van Langenhove, H., 2015. Quantification of
609 PAHs and oxy-PAHs on airborne particulate matter in Chiang Mai, Thailand, using gas chromatography high resolution
610 mass spectrometry. *Atmos. Environ.* 107, 262–272. <https://doi.org/10.1016/j.atmosenv.2015.02.051>

611 Walgraeve, C., De Wispelaere, P., Van der Elst, F., Van Langenhove, H., 2017. Development of an analytical method to
612 determine oxy-PAHs and PAHs in *Taxus baccata* leaves. *Anal. Bioanal. Chem.* 409, 335–347.
613 <https://doi.org/10.1007/s00216-016-0008-9>

614 Walgraeve, C., Demeestere, K., Dewulf, J., Zimmermann, R., Van Langenhove, H., 2010. Oxygenated polycyclic aromatic
615 hydrocarbons in atmospheric particulate matter: Molecular characterization and occurrence. *Atmos. Environ.* 44,
616 1831–1846. <https://doi.org/10.1016/j.atmosenv.2009.12.004>

617 Wania, F., Haugen, J.E., Lei, Y.D., Mackay, D., 1998. Temperature dependence of atmospheric concentrations of semivolatile
618 organic compounds. *Environ. Sci. Technol.* 32, 1013–1021. <https://doi.org/10.1021/es970856c>

619 World Health Organisation, 2021. Human health effects of polycyclic aromatic hydrocarbons as ambient air pollutants: report
620 of the working group on polycyclic aromatic hydrocarbons of the joint task force on the health aspects of air Pollution.

621 Yang, R., Xie, T., Li, A., Yang, H., Turner, S., Wu, G., Jing, C., 2016. Sedimentary records of polycyclic aromatic hydrocarbons
622 (PAHs) in remote lakes across the Tibetan Plateau. *Environ. Pollut.* 214, 1–7.
623 <https://doi.org/10.1016/j.envpol.2016.03.068>

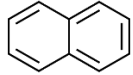
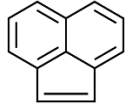
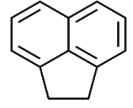
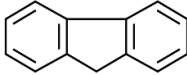
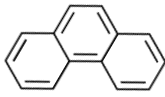
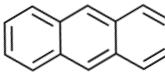
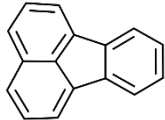
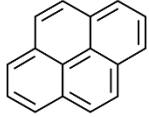
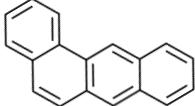
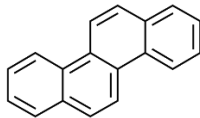
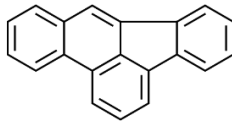
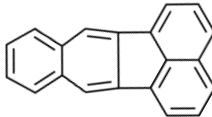
624 Yao, Y., Meng, X.Z., Wu, C.C., Bao, L.J., Wang, F., Wu, F.C., Zeng, E.Y., 2016. Tracking human footprints in Antarctica through
625 passive sampling of polycyclic aromatic hydrocarbons in inland lakes. *Environ. Pollut.* 213, 412–419.
626 <https://doi.org/10.1016/j.envpol.2016.02.035>

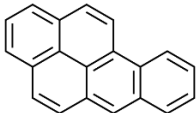
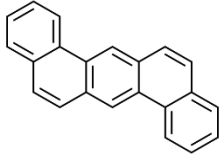
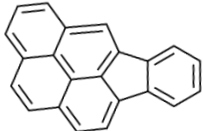
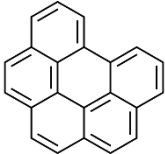
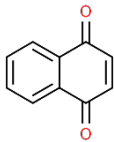
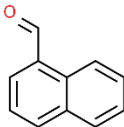
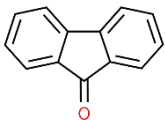
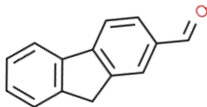
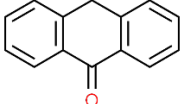
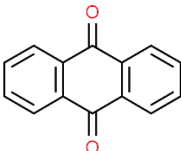
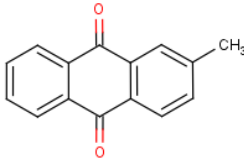
627 Zhang, Xue, Zhang, Z.F., Zhang, Xianming, Zhu, F.J., Li, Y.F., Cai, M., Kallenborn, R., 2021. Polycyclic Aromatic Hydrocarbons
628 in the Marine Atmosphere from the Western Pacific to the Southern Ocean: Spatial Variability, Gas/Particle
629 Partitioning, and Source Apportionment. *Environ. Sci. Technol.* <https://doi.org/10.1021/acs.est.1c08429>

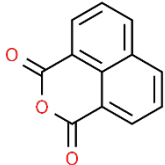
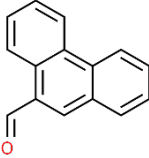
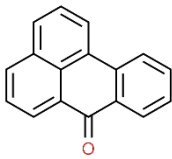
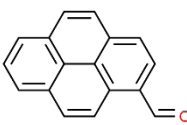
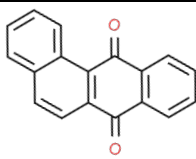
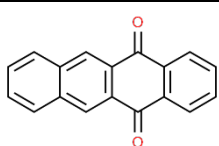
630

631

632 **Supplementary Information**
633 **S.I. 1: Structural formula of the PAHs and oxy-PAHs discussed in this study**

Structural formula	IUPAC Name (Synonym)	CAS	Molecular formula	Molecular mass
	Naphthalene	91-20-3	C ₁₀ H ₈	128.17
	Acenaphthylene	208-96-8	C ₁₂ H ₈	152.19
	Acenaphthene	83-32-9	C ₁₂ H ₁₀	154.21
	Fluorene	86-73-7	C ₁₃ H ₁₀	166.22
	Phenanthrene	85-01-8	C ₁₄ H ₁₀	178.23
	Anthracene	120-12-7	C ₁₄ H ₁₀	178.23
	Fluoranthene	206-44-0	C ₁₆ H ₁₀	202.25
	Pyrene	129-00-0	C ₁₆ H ₁₀	202.25
	Benz[a]anthracene	56-55-3	C ₁₈ H ₁₂	228.28
	Chrysene	218-01-9	C ₁₈ H ₁₂	228.29
	Benzo[b]fluoranthene	205-99-2	C ₂₀ H ₁₂	252.31
	Benzo[k]fluoranthene	207-08-9	C ₂₀ H ₁₂	252.31

	Benzo[<i>a</i>]pyrene	50-32-8	C ₂₀ H ₁₂	252.31
	Dibenz[<i>a,h</i>]anthracene	53-70-3	C ₂₂ H ₁₄	278.35
	Indeno[1,2,3- <i>cd</i>]pyrene	193-39-5	C ₂₂ H ₁₂	276.33
	Benzo[<i>ghi</i>]perylene	191-24-2	C ₂₂ H ₁₂	276.33
	1,4-Naphthoquinone (1,4-Naphthalenedione)	130-15-4	C ₁₀ H ₆ O ₂	158.15
	1-Naphthaldehyde (1-Naphthalenecarboxaldehyde)	66-77-3	C ₁₁ H ₈ O	156.18
	9 <i>H</i> -Fluoren-9-one (9-Fluorenone)	486-25-9	C ₁₃ H ₈ O	180.20
	9 <i>H</i> -Fluorene-2-carbaldehyde (Fluorene-2-carboxaldehyde)	30084-90-3	C ₁₄ H ₁₀ O	194.23
	9(10 <i>H</i>)-Anthracenone (Anthracen-9-one)	90-44-8	C ₁₄ H ₁₀ O	194.23
	9,10-Anthraquinone (9,10-Anthracenedione)	84-65-1	C ₁₄ H ₈ O ₂	208.21
	2-Methylanthraquinone	84-54-8	C ₁₅ H ₁₀ O ₂	222.24

	1 <i>H</i> ,3 <i>H</i> -Benzo[<i>de</i>]isochromene-1,3-dione (1,8-Naphthalic anhydride)	81-84-5	C ₁₂ H ₆ O ₃	198.17
	9-Phenanthrenecarbaldehyde (9-Phenanthrenecarboxaldehyde)	4707-71-5	C ₁₅ H ₁₀ O	206.24
	7 <i>H</i> -Benzo[<i>de</i>]anthracen-7-one (Benzanthrone)	82-05-3	C ₁₇ H ₁₀ O	230.26
	1-Pyrenecarbaldehyde (Pyrene-1-carboxaldehyde)	3029-19-4	C ₁₇ H ₁₀ O	230.26
	7,12-Tetraphenedione (Benz[<i>a</i>]anthracene-7,12-dione)	2498-66-0	C ₁₈ H ₁₀ O ₂	258.27
	5,12-Tetracenedione (5,12-Naphthacenedione)	1090-13-7	C ₁₈ H ₁₀ O ₂	258.27

635

S.I. 2: Composition of the used PAH standard

Compound	Concentration (ng/mL)	Supplier and Quality
Naphthalene	1000	Chiron S-4063-100-5T
Acenaphthylene	1000	Chiron S-4063-100-5T
Acenaphthene	1000	Chiron S-4063-100-5T
Fluorene	1000	Chiron S-4063-100-5T
Phenanthrene	1000	Chiron S-4063-100-5T
Anthracene	1000	Chiron S-4063-100-5T
Fluoranthene	1000	Chiron S-4063-100-5T
Pyrene	1000	Chiron S-4063-100-5T
Benz[a]anthracene	1000	Chiron S-4063-100-5T
Chrysene	1000	Chiron S-4063-100-5T
Benzo[b]fluoranthene	1000	Chiron S-4063-100-5T
Benzo[k]fluoranthene	1000	Chiron S-4063-100-5T
Benzo[a]pyrene	1000	Chiron S-4063-100-5T
Dibenz[a,h]anthracene	1000	Chiron S-4063-100-5T
Benzo[ghi]perylene	1000	Chiron S-4063-100-5T
Indeno[1,2,3-cd]pyrene	1000	Chiron S-4063-100-5T
Naphtalene-d8	400	Chiron S-4124-200-T
Biphenyl-d10	400	Chiron S-4124-200-T
Phenanthrene-d10	400	Chiron S-4124-200-T
Pyrene-d10	400	Chiron S-4124-200-T
Benz[a]anthracene-d12	400	Chiron S-4124-200-T
Benzo[a]pyrene-d12	400	Chiron S-4124-200-T
Benzo[ghi]perylene-d12	402	Chiron S-4124-200-T

636

637

638

S.I. 3: Composition of the used oxy-PAH standard

Compound	Concentration (ng/mL)	Supplier and quality
1,4-Naphthoquinone	402	Acros Organics (99%)
Naphthalene-1-carboxaldehyde	480	Acros Organics (95%)
9-Fluorenone	494	Merck Life Science (98%)
Fluorene-2-carboxaldehyde	416	Merck Life Science (99%)
Anthracene-9-one	388	Acros Organics (97%)
Anthraquinone	528	Merck Life Science (97%)
2-Methylanthraquinone	396	Merck Life Science (95%)
1,8-Naphthalic anhydride	420	Acros Organics (97%)
Phenanthrene-9-carbaldehyde	384	Merck Life Science (97%)
Benzanthrone	430	Merck Life Science (99%)
1-Pyrenecarboxaldehyde	396	Merck Life Science (99%)
Benz[a]anthracene-7,12-dione	382	Acros Organics (99%)
5,12-Naphthacenequinone	408	Acros Organics (97%)
Naphtalene-d8	400	Chiron S-4124-200-T
Biphenyl-d10	400	Chiron S-4124-200-T
Phenanthrene-d10	400	Chiron S-4124-200-T
Pyrene-d10	400	Chiron S-4124-200-T
Benz[a]anthracene-d12	400	Chiron S-4124-200-T
Benzo[a]pyrene-d12	400	Chiron S-4124-200-T
Benzo[ghi]perylene-d12	402	Chiron S-4124-200-T

639

640

S.I. 4: Sampling location; the Princess Elisabeth station

The station is constructed in 2009 on a granite ridge (Utsteinen ridge), which is 700 m long, oriented on the North-South axis, and protruding about 20 m above the snow surface (Pattyn et al., 2009). A map showing the surroundings of the station is shown in Figure 1. The station is built following a zero-emission concept as it relies on renewable energy sources (wind, solar, PV) for its operation. Because of this, local emissions of organic pollutants are limited. As the station is only manned during the austral summer (November-February), active high-volume sampling is conducted during these months. The high-volume sampler (see Section 2.3) was installed in an insulated container unit, clad with stainless steel sheets, and anchored 350 m north from the station on the same ridge. The station's area is characterized by a relatively mild microclimate as it is sheltered from the cold air from the plateau by the nearby mountain range (Sør Rondane). The primary wind direction at the station is east which is associated with warmer synoptic regimes. Winds with a southern component (SE-SSE) are mostly of katabatic origin (Gorodetskaya et al., 2015). Detailed meteorological parameters such as air temperature, relative humidity, wind speed/direction, snowfall and accumulation were studied near the station and reported by (Souverijns et al., 2018) and (Gorodetskaya et al., 2013).

S.I. 5: ASE 350 maintenance and quality management

The extraction cells, 66 mL zirconium alloy (Zr) and stainless steel (SST) 22 mL, were outfitted with PTFE O-rings, PEEK washers and stainless-steel frits. Cells were frequently (every 25 cycles) rebuilt by replacing consumables (O-rings, washers, and frits) and cleaning with acetone in an ultrasonic bath before drying in an oven at 100°C. Between consecutive sample extractions, the PLE cells were cleaned using method Cond. 1 from Table 1. Extracts were collected in 250 mL glass bottles which were washed in a laboratory dishwasher and subsequently dried in an oven at 200°C for at least 24 hours, after which they were capped using PTFE-lined silicon septa and a PLE compatible cap.

S.I. 6: Formula used to calculate the flow of the high-volume sampler at standard conditions

$$Q_s = Q_m \times \frac{T_N}{p_N} \times \sqrt{\frac{(p_{ref} \times p_m)}{(T_{ref} \times T_m)}}$$

Q_m = measured flow rate (500 L.min⁻¹), T_N and p_N ; temperature and pressure at normal conditions 298K and 1013 Pa, T_{ref} and p_{ref} ; temperature and pressure at which the flowmeter was calibrated

S.I. 7: Description of the GC-MS method for the PAH and oxy-PAH method

Each run, 1 µL of the extract was injected on a BEST PTV injector (Interscience, Louvain-la-Neuve, Belgium) equipped with a Topaz 2.0 mm I.D. baffled inlet liner (Restek, USA) in splitless mode. The solvent was evaporated during 1 min at 35 °C after which the temperature was increased to 320°C at a rate of 14.5 °C/s and held for 5 min. Helium was used as a carrier gas at a flow rate of 1 mL/min. Only for the oxy-PAHs a ramped pressure to 150 kPa was used during the injection phase. The GC oven was kept at 70°C for 2.5 min after injection, then the temperature was increased at a rate of 10 °C/min until 320°C was reached and held for 15 min. The MS transfer line was heated to 290 °C. The separated compounds were ionized using electron ionization (EI; 70 eV). The mass spectrometer was run in multiple ion detection mode (MID) with a mass resolving power above 10.000 (10% valley definition). Perfluoro-kerosene gives at least 2 fragments in each MID window (lock and calibration ion) and was used as internal reference to calibrate accurate masses.

S.I. 8: Sample treatment before applying Positive matrix factorization

PMF is a multivariate factor analysis (FA) tool used to model source contribution. It overcomes limitations of principal component analysis (PCA) by eliminating negative contributions to the model and incorporating experimental uncertainties. For environmental samples better model performance was found compared to other FA tools. Compounds with a signal-to-noise ratio, calculated from the compounds concentration and uncertainty, < 0.5 were excluded from the dataset and for those with a weak S/N (0.5-2) the uncertainty was increased with a factor 3 as recommended by (U.S. Environmental Protection Agency, 2014). Values below MDL, MQL or IDL were substituted by MDL/2, MQL/2, and IDL/2. The error matrix was constructed by estimating setting a 10% error for each data point as MDL_i + 0.1 x C_i for measurements above MDL and 5/6 x MDL for values below MDL. The base model ran 20 times for 3 to 8 factors, each time the outcome with the lowest Q was evaluated with 100 bootstrap runs.

697

698

S.I. 9: MID windows for the PAH GC-HRMS method

	Retention time (min)	Compound	Mass (a.m.u.)	Measurement time (ms)
Window 1				
Start Time:	7.5	Naphthalene	128.062	147
Measure Time:	2.5	Lock	130.991	36
End Time:	10	Naphthalene-d8	136.112	24
		Cali	168.988	73
Window 2				
Start Time:	10	Biphenyl-d10	164.14	27
Measure Time:	1.8	Lock	168.988	73
End Time:	11.8	Cali	192.988	110
Window 3:				
Start Time:	11.8	Lock	130.991	23
Measure Time:	3.99	Acenaphthylene	152.062	92
End Time:	15.79	Acenaphthene	153.07	92
		Fluorene	166.078	92
		Cali	168.988	46
Window 4				
Start Time:	15.79	Lock	168.988	26
Measure Time:	2.21	Phenanthrene/Anthracene	178.078	104
End Time:	18	Phenanthrene-d10	188.14	26
		Cali	192.988	104
Window 5				
Start Time:	18	Lock	180.988	96
Measure Time:	2.6	Fluoranthene/Pyrene	202.078	96
End Time:	20.6	Pyrene-d10	212.140	32
		Cali	218.985	32
Window 6				
Start Time:	20.6	Benz[a]anthracene/Chrysene	228.093	122
Measure Time:	4.3	Lock	230.985	61
End Time:	24.9	Benz[a]anthracene-d12	240.169	24
		Cali	280.982	61
Window 7				
Start Time:	24.9	Lock	230.985	48
Measure Time:	1.85	Benzo[b]fluoranthene/Benzo[k]fluoranthene	252.093	97
End Time:	26.75	Cali	280.982	97
Window 8				
Start Time:	26.75	Lock	230.985	65
Measure Time:	1.75	Benzo[a]pyrene	252.093	131
End Time:	28.5	Benzo[a]pyrene-d12	264.169	26
		Cali	280.982	65
Window 9:				
Start Time:	28.5	Lock	230.985	65
Measure Time:	14	Indeno[1,2,3-cd]pyrene/Benzo[ghi]perylene	276.093	65
End Time:	42.5	Dibenz[a,h]anthracene	278.109	65
		Cali	280.982	65
		Benzo[ghi]perylene-d12	288.169	21

699

700

701

S.I. 10: MID windows for the oxy-PAH GC-HRMS method

	Retention time (min)	Compound	Mass (a.m.u.)	Measurement time (ms)
Window 1				
Start Time:	10	Lock	130.991	27
Measure Time:	5.5	1-Naphthalenecarboxaldehyde	156.057	108
End Time:	15.5	1,4-Naphthalenedione	158.036	108
		Biphenyl-d10	164.140	36
		Cali	168.988	54
Window 2:				
Start Time:	15.5	Lock	168.988	35
Measure Time:	2.5	9-Fluorenone	180.057	140
End Time:	18	Phenanthrene-d10	188.140	70
		Cali	192.988	70
Window 3				
Start Time:	18	Lock	180.988	52
Measure Time:	1.9	Fluorene-2-carboxaldehyde/Anthracene-9-one	194.073	105
End Time:	19.9	9,10-Anthracenedione	208.052	105
		Cali	218.985	52
Window 4				
Start Time:	19.9	Lock	180.988	29
Measure Time:	2.72	1,8-Naphthalic anhydride	198.031	88
End Time:	22.62	9-Phenanthrenecarboxaldehyde	206.073	88
		Pyrene-d10	212.140	29
		Cali	218.985	29
		2-Methylantraquinone	222.068	88
Window 5:				
Start Time:	22.62	Benzanthrone/Pyrene-1-carboxaldehyde	230.073	100
Measure Time:	4.38	Lock	230.985	33
End Time:	27	Benz[<i>a</i>]anthracene-d12	240.169	50
		Benz[<i>a</i>]anthracene-7,12-dione/5,12-Naphthacenedione	258.068	100
		Cali	280.982	50

702

703

704 S.I. 11: Quality control parameters and MS variables

	IDL (ng) 95% C.I. (n=3)	Interday precision (RSD%) (n=4)	Intraday precision (RSD%) (n=4)	RRF (n=3)	Linearity (n=3) (R ²)	t _r (min)	(M) ⁺	R1 (lock ion)	R2 (cali ion)	Internal Standard
Napthalene	0.47	0.7	1.3	0.968	1.000	9.30	128.0620	130.992	168.988	Napthalene-d8
Acenaphthylene	0.20	2.1	2.8	0.517	1.000	13.45	152.0620	130.992	168.988	Biphenyl-d10
Acenaphthene	0.15	1.5	0.7	0.319	1.000	13.78	153.0699	130.992	168.988	Biphenyl-d10
Fluorene	0.17	2.1	3.7	0.393	1.000	15.00	166.0777	130.992	168.988	Phenanthrene-d10
Phenanthrene	0.13	0.2	0.5	1.044	1.000	17.73	178.0777	168.988	192.988	Phenanthrene-d10
Anthracene	0.09	0.2	2.3	0.925	1.000	17.80	178.0777	168.988	192.988	Phenanthrene-d10
Fluoranthene	0.16	1.1	2.0	0.914	1.000	20.85	202.0777	180.988	218.985	Pyrene-d10
Pyrene	0.21	0.6	1.5	1.017	1.000	21.55	202.0777	180.988	218.985	Pyrene-d10
Benz[a]anthracene	0.48	0.3	2.2	1.022	1.000	24.60	228.0931	230.985	280.982	Benz[a]anthracene-d12
Chrysene	0.06	1.6	2.2	1.097	1.000	24.80	228.0931	230.985	280.982	Benz[a]anthracene-d12
Benzo[b]fluoranthene	0.43	2.1	4.0	1.010	1.000	27.28	252.0933	230.985	280.982	Benzo[a]pyrene-d12
Benzo[k]fluoranthene	0.34	0.6	3.2	1.241	0.997	27.33	252.0933	230.985	280.982	Benzo[a]pyrene-d12
Benzo[a]pyrene	0.25	0.8	0.6	1.031	1.000	28.30	252.0933	230.985	280.982	Benzo[a]pyrene-d12
Dibenz[a,h]anthracene	0.24	1.7	1.7	0.810	1.000	31.65	278.1090	230.985	280.982	Benzo[ghi]perylene-d12
Indeno[1,2,3-cd]pyrene	0.07	1.9	2.3	1.009	0.999	31.65	276.0930	230.985	280.982	Benzo[ghi]perylene-d12
Benzo[ghi]perylene	0.84	1.0	2.8	0.861	1.000	33.05	276.0930	230.985	280.982	Benzo[ghi]perylene-d12
Napthalene-1,4-dione	0.24	4.2	3.3	0.133	0.999	13.55	158.0362	130.992	168.988	Biphenyl-d10
Napthalene-1-carboxaldehyde	0.19	7.7	2.9	0.193	0.999	14.60	156.0570	130.992	168.988	Biphenyl-d10
Fluorene-9-one	0.51	1.2	6.4	0.417	1.000	17.40	180.0570	168.988	192.988	Phenanthrene-d10
Fluorene-2-carboxaldehyde	0.19	4.0	3.2	0.087	0.996	19.85	194.0726	180.988	218.985	Phenanthrene-d10
Anthracene-9-one	0.17	47.2	23.0	0.111	0.967	19.95	194.0726	180.988	218.985	Phenanthrene-d10
Anthracene-9,10-dione	0.23	3.1	2.8	0.132	0.999	20.23	208.0519	180.988	218.985	Phenanthrene-d10
2-Methylanthraquinone	0.73	6.6	2.7	0.086	0.999	21.40	222.0675	180.988	218.985	Phenanthrene-d10
1,8-naphthalic anhydride	1.23	1.9	4.1	0.051	0.999	21.50	198.0311	180.988	218.985	Pyrene-d10
Phenanthrene-9-carboxaldehyde	0.18	1.1	1.9	0.141	1.000	21.80	206.0726	180.988	218.985	Pyrene-d10
7H-benzo[de]anthracene-7-one	0.17	6.3	2.6	0.211	0.999	25.50	230.0725	230.985	280.982	Benz[a]anthracene-d12
Pyrene-1-carboxaldehyde	0.45	4.7	7.3	0.207	1.000	25.55	230.0725	230.985	280.982	Benz[a]anthracene-d12
Benz[a]anthracene-7,12-dione	0.46	7.5	2.6	0.111	0.998	26.05	258.0675	230.985	280.982	Benz[a]anthracene-d12
5,12-Naphthacenequinone	1.08	4.3	0.4	0.136	1.000	26.80	258.0675	230.985	280.982	Benzo[a]pyrene-d12

705

706

707

708
709

S.I. 12: Average (n=3) experimental analyte recovery of the measured PAHs and oxy-PAHs in % of spiked compound mass.

	PUF mean recovery (%) (n=3)	RSD (%)	QFF Mean recovery (%) (n=3)	RSD (%)
Naphthalene	68	7	142	9
Acenaphthylene	78	3	131	7
Acenaphthene	78	1	68	12
Fluorene	74	2	52	19
Phenanthrene	78	3	82	5
Anthracene	98	5	111	10
Fluoranthene	95	4	72	5
Pyrene	91	3	73	4
Benz[<i>a</i>]anthracene	93	6	70	6
Chrysene	89	5	97	2
Benzo[<i>b</i>]fluoranthene	102	9	71	10
Benzo[<i>k</i>]fluoranthene	88	8	70	8
Benzo[<i>a</i>]pyrene	95	6	67	7
Dibenz[<i>a,h</i>]anthracene	101	6	Not in SRM	
Indeno[1,2,3- <i>cd</i>]pyrene	97	5	85	4
Benzo[<i>ghi</i>]perylene	96	5	87	2
Napthalene-1,4-dione	54	9	40	11
Napthalene-1-carboxaldehyde	98	16	86	7
Fluorene-9-one	113	15	84	4
Fluorene-2-carboxaldehyde	123	23	109	4
Anthracene-9-one	21	8	33	44
Anthracene-9,10-dione	143	14	108	5
2-Methylanthraquinone	118	17	124	3
1,8-naphthalic anhydride	120	7	16	10
Phenanthrene-9-carboxaldehyde	106	20	93	3
Benzanthrone	118	10	124	8
Pyrene-1-carboxaldehyde	97	16	80	7
Benz[<i>a</i>]anthracene-7,12-dione	104	18	77	5
5,12-Naphthacenequinone	123	10	144	13

710

711 S.I. 13: Concentration (pg m⁻³) of PAHs in the gas phase measured from 2017 to 2021 at the Princess Elisabeth Station, Antarctica

Sample start	13/12/17	20/12/17	27/12/17	03/01/18	10/01/18	17/01/18	25/01/18	06/02/18	01/12/18	08/12/18	17/12/18	01/01/19	08/01/19	17/01/19
Sample stop	20/12/17	27/12/17	03/01/18	10/01/18	17/01/18	25/01/18	01/02/18	09/02/18	08/12/18	15/12/18	24/12/18	08/01/19	17/01/19	24/01/19
Naphthalene	<MDL	<MDL	<MQL	11.91	<MQL	15.08	<MQL	<MQL	10.38	9.46	17.05	<MQL	<MDL	97.45
Acenaphthylene	0.62	0.45	0.4	0.64	0.92	10.48	14	4.24	8.28	1.07	4.51	0.7	0.81	3.38
Acenaphthene	N.D.	0.78	0.64	2	2.27	1.44	1.79	N.D.	1.25	0.94	1.46	N.D.	N.D.	11.3
Fluorene	2.61	1.7	1.2	6.07	11.61	4.93	3.45	1.68	2.55	3.46	5.77	2.5	2.1	18.3
Phenanthrene	51.91	21.57	11.46	22.45	22.34	29.98	23.41	9.97	26.4	9.74	20.01	6.73	7.67	27.9
Anthracene	1.45	1.14	0.51	1.12	1.11	0.67	0.51	0.41	0.39	0.43	0.73	<MQL	0.4	0.91
Fluoranthene	37.13	55.86	7.43	10.3	5.93	10.72	13.96	9.54	27.67	6.82	7.68	2.21	1.83	3.53
Pyrene	25.24	38.16	4.22	7.92	4.29	8.09	8.88	5.12	16.98	2.71	3.12	1.11	1.02	2.83
Benz[a]anthracene	N.D.	N.D.	N.D.	<MDL	N.D.	N.D.	N.D.	N.D.	N.D.	N.D.	N.D.	N.D.	N.D.	N.D.
Chrysene	0.33	1.98	0.4	1.75	0.36	0.53	0.3	0.33	0.3	0.15	0.24	0.15	0.19	0.24
Benzo[b]fluoranthene	<MDL	0.31	<MQL	0.39	<MQL	<MQL	<MQL	<MDL	<MDL	N.D.	<MDL	<MDL	<MDL	<MDL
Benzo[k]fluoranthene	<MDL	<MDL	N.D.	<MQL	<MDL	<MDL	<MDL	<MDL	<MDL	N.D.	<MDL	<MDL	<MDL	<MDL
Benzo[a]pyrene	N.D.	N.D.	N.D.	<MDL	<MDL	N.D.	N.D.	N.D.	N.D.	N.D.	N.D.	N.D.	N.D.	N.D.
Dibenz[a,h]anthracene	N.D.	N.D.	N.D.	<MDL	<MDL	<MDL	<MDL	N.D.	N.D.	N.D.	N.D.	N.D.	N.D.	N.D.
Indeno[1,2,3-cd]pyrene	N.D.	N.D.	N.D.	<MDL	<MDL	<MDL	N.D.	N.D.	N.D.	N.D.	N.D.	N.D.	N.D.	N.D.
Benzo[ghi]perylene	N.D.	N.D.	N.D.	<MDL	<MDL	<MDL	<MDL	N.D.	N.D.	N.D.	N.D.	N.D.	N.D.	N.D.

Sample start	27/11/19	04/12/19	11/12/19	18/12/19	25/12/19	01/01/20	08/01/20	15/01/20	22/01/20	29/01/20	07/12/20	15/12/20	23/12/20	31/12/20	08/01/21	15/01/21	22/01/21	29/01/21
Sample stop	04/12/19	11/12/19	18/12/19	25/12/19	01/01/20	08/01/20	15/01/20	22/01/20	29/01/20	05/02/20	15/12/20	23/12/20	30/12/20	08/01/21	15/01/21	22/01/21	29/01/21	05/02/21
Naphthalene	<MDL	<MQL	<MDL	19.52	<MQL	<MDL	<MDL	<MQL	<MDL	<MDL	<MDL	<MDL	16.92	<MQL	30.79	<MDL	<MDL	<MDL
Acenaphthylene	N.D.	2.23	N.D.	1.56	N.D.	1.32	N.D.	N.D.	N.D.	N.D.	0.53	2.04	18.21	1.71	2.95	0.7	0.43	1.77
Acenaphthene	<MQL	0.58	N.D.	1.45	<MDL	N.D.	<MQL	N.D.	N.D.	N.D.	<MQL	<MQL	2.53	1.08	2.02	<MQL	<MDL	<MQL
Fluorene	1.34	1	1.56	2.93	<MQL	1.13	1.15	3.13	3.14	1.08	1.25	5.47	7.07	6.1	6.17	2.22	<MQL	2.46
Phenanthrene	11.5	4.52	10.59	8.16	3.81	5.08	4.11	8.7	10.03	4.54	3.45	11.6	13.28	34.64	7.77	5.03	2.27	5.13
Anthracene	0.32	0.31	0.32	0.54	0.35	0.39	0.26	0.53	0.47	0.33	<MQL	<MQL	0.57	N.D.	<MDL	0.23	<MQL	<MQL
Fluoranthene	3.8	1.48	2.12	1.78	0.97	1.1	1.51	1.62	1.31	1.03	0.94	2.11	2.13	7.24	2.29	1.76	0.92	1.28
Pyrene	3.03	1.03	1.23	1.39	0.76	0.86	0.69	1.41	1.91	1.11	1.42	2.66	3.83	3.86	1.62	1.29	1.49	3.25
Benz[a]anthracene	N.D.	N.D.	N.D.	N.D.	N.D.	N.D.	N.D.	N.D.	N.D.	N.D.	<MDL	<MDL	<MDL	<MDL	<MDL	<MDL	<MDL	<MDL
Chrysene	0.07	0.13	0.11	0.17	0.12	0.1	0.08	N.D.	N.D.	N.D.	N.D.	N.D.	N.D.	N.D.	N.D.	N.D.	N.D.	N.D.
Benzo[b]fluoranthene	<MDL	<MDL	<MDL	<MDL	<MDL	<MDL	<MDL	<MDL	<MDL	<MDL	<MDL	<MDL	<MDL	<MDL	<MDL	<MDL	<MDL	N.D.
Benzo[k]fluoranthene	<MDL	<MDL	<MDL	<MDL	<MDL	<MDL	<MDL	<MDL	<MDL	<MDL	<MDL	<MDL	<MDL	<MDL	<MDL	<MDL	<MDL	N.D.
Benzo[a]pyrene	<MDL	<MDL	<MDL	N.D.	<MDL	N.D.	N.D.	N.D.	<MDL	N.D.	<MQL	<MDL	<MDL	<MDL	N.D.	N.D.	N.D.	N.D.
Dibenz[a,h]anthracene	<MDL	N.D.	N.D.	N.D.	N.D.	N.D.	N.D.	N.D.	N.D.	N.D.	<MDL	<MDL	<MDL	N.D.	N.D.	N.D.	N.D.	N.D.
Indeno[1,2,3-cd]pyrene	N.D.	N.D.	N.D.	N.D.	N.D.	N.D.	N.D.	N.D.	N.D.	N.D.	<MQL	<MQL	<MQL	<MDL	<MDL	<MDL	<MDL	N.D.
Benzo[ghi]perylene	N.D.	N.D.	N.D.	N.D.	N.D.	N.D.	N.D.	N.D.	N.D.	N.D.	<MQL	<MQL	<MDL	<MDL	<MDL	<MDL	<MQL	<MDL

712

713

714 S.I. 14: Concentration (pg m⁻³) of PAHs in the particle phase measured from 2017 to 2021 at the Princess Elisabeth Station, Antarctica

Sample start	13/12/17	20/12/17	27/12/17	03/01/18	10/01/18	17/01/18	25/01/18	06/02/18	01/12/18	08/12/18	17/12/18	01/01/19	08/01/19	17/01/19
Sample stop	20/12/17	27/12/17	03/01/18	10/01/18	17/01/18	25/01/18	01/02/18	09/02/18	08/12/18	15/12/18	24/12/18	08/01/19	17/01/19	24/01/19
Acenaphthylene	N.D.	N.D.	N.D.	N.D.	N.D.	N.D.	N.D.	N.D.	0.15	N.D.	N.D.	N.D.	N.D.	N.D.
Acenaphthene	0.66	N.D.	N.D.	N.D.	N.D.	N.D.	N.D.	N.D.	1.7	N.D.	N.D.	N.D.	N.D.	N.D.
Fluorene	<MQL	N.D.	0.23	N.D.	N.D.	N.D.	0.36	N.D.	0.6	0.28	<MQL	N.D.	N.D.	N.D.
Phenanthrene	N.D.	<MQL	1.39	<MQL	<MQL	N.D.	<MQL	N.D.	N.D.	<MDL	<MDL	<MDL	<MDL	<MDL
Anthracene	N.D.	N.D.	N.D.	N.D.	N.D.	N.D.	N.D.	N.D.	N.D.	N.D.	N.D.	N.D.	N.D.	N.D.
Fluoranthene	0.33	0.51	2.36	0.31	0.4	0.21	0.3	<MQL	0.2	<MDL	0.32	<MDL	<MDL	<MDL
Pyrene	0.43	0.49	1.62	0.43	0.37	0.24	0.34	0.57	<MQL	<MDL	0.14	<MDL	<MDL	<MDL
Benz[a]anthracene	N.D.	0.4	0.99	N.D.	N.D.	<IDL	<IDL	N.D.	N.D.	N.D.	<IDL	<IDL	N.D.	N.D.
Chrysene	N.D.	1.02	1.29	N.D.	0.28	N.D.	N.D.	N.D.	N.D.	N.D.	N.D.	N.D.	N.D.	N.D.
Benzo[b]fluoranthene	0.34	2.27	1.82	0.46	0.4	0.75	<MQL	<MDL	<MDL	<MDL	0.49	<MDL	<MDL	<MDL
Benzo[k]fluoranthene	<MQL	0.59	0.6	<MQL	<MDL	<MQL	N.D.	N.D.	N.D.	<MDL	<MQL	<MDL	<MDL	<MDL
Benzo[a]pyrene	0.09	0.47	0.78	0.12	N.D.	N.D.	N.D.	N.D.	N.D.	N.D.	<IDL	<IDL	N.D.	<IDL
Dibenz[a,h]anthracene	<MDL	<MDL	<MQL	N.D.	N.D.	<MDL	N.D.	N.D.	N.D.	<MDL	<MDL	<MDL	<MDL	N.D.
Indeno[1,2,3-cd]pyrene	0.28	1.26	0.82	0.29	<MQL	0.32	<MDL	<MDL	N.D.	N.D.	<MQL	<MDL	N.D.	<MDL
Benzo[ghi]perylene	0.48	1.93	0.98	0.56	0.22	0.45	<MDL	<MDL	N.D.	<MDL	0.35	<MDL	<MDL	N.D.

Sample start	27/11/19	04/12/19	11/12/19	18/12/19	25/12/19	01/01/20	08/01/20	15/01/20	22/01/20	29/01/20	07/12/20	15/12/20	23/12/20	31/12/20	08/01/21	15/01/21	22/01/21	29/01/21
Sample stop	04/12/19	11/12/19	18/12/19	25/12/19	01/01/20	08/01/20	15/01/20	22/01/20	29/01/20	05/02/20	15/12/20	23/12/20	30/12/20	08/01/21	15/01/21	22/01/21	29/01/21	05/02/21
Acenaphthylene	N.D.	N.D.	N.D.	N.D.	N.D.	N.D.	N.D.	N.D.	N.D.	N.D.	N.D.	N.D.	N.D.	N.D.	N.D.	N.D.	N.D.	N.D.
Acenaphthene	N.D.	N.D.	N.D.	N.D.	N.D.	N.D.	N.D.	N.D.	N.D.	N.D.	N.D.	N.D.	N.D.	N.D.	N.D.	N.D.	N.D.	N.D.
Fluorene	N.D.	N.D.	N.D.	N.D.	N.D.	<MQL	N.D.	N.D.	<MQL	N.D.	<MDL	<MDL	0.73	<MQL	<MDL	<MDL	0.37	<MQL
Phenanthrene	<MDL	<MDL	<MDL	<MDL	<MDL	<MQL	<MDL	<MDL	<MQL	<MDL	<MDL	<MDL	<MQL	N.D.	<MDL	<MDL	1.37	<MQL
Anthracene	N.D.	N.D.	N.D.	N.D.	N.D.	N.D.	N.D.	N.D.	N.D.	N.D.	N.D.	N.D.	N.D.	N.D.	N.D.	N.D.	N.D.	N.D.
Fluoranthene	<MQL	<MDL	<MDL	<MQL	<MDL	<MQL	<MDL	<MDL	0.69	<MDL	0.18	0.74	0.69	<MQL	<MQL	<MQL	0.64	0.35
Pyrene	0.29	0.17	0.27	<MQL	0.33	<MQL	0.19	<MDL	0.73	0.31	<MDL	1.92	1.28	<MQL	<MDL	<MDL	0.22	0.28
Benz[a]anthracene	<IDL	N.D.	N.D.	N.D.	N.D.	<IDL	N.D.	N.D.	N.D.	N.D.	N.D.	N.D.	N.D.	N.D.	N.D.	N.D.	N.D.	N.D.
Chrysene	N.D.	N.D.	N.D.	N.D.	N.D.	N.D.	N.D.	N.D.	N.D.	N.D.	N.D.	N.D.	N.D.	N.D.	N.D.	N.D.	N.D.	N.D.
Benzo[b]fluoranthene	<MDL	<MDL	<MDL	<MDL	<MDL	N.D.	<MDL	<MDL	<MDL	<MDL	N.D.	N.D.	<MQL	N.D.	N.D.	N.D.	<MQL	N.D.
Benzo[k]fluoranthene	<MDL	N.D.	<MDL	<MDL	N.D.	N.D.	<MDL	<MDL	<MDL	<MDL	N.D.	N.D.	<MDL	N.D.	N.D.	N.D.	<MDL	N.D.
Benzo[a]pyrene	N.D.	N.D.	<IDL	N.D.	<IDL	N.D.	N.D.	N.D.	<IDL	N.D.	N.D.	N.D.	N.D.	N.D.	N.D.	N.D.	N.D.	N.D.
Dibenz[a,h]anthracene	<MDL	N.D.	<MDL	N.D.	<MDL	N.D.	<MDL	N.D.	N.D.	<MDL	<MDL	<MDL	N.D.	<MDL	N.D.	N.D.	<MDL	N.D.
Indeno[1,2,3-cd]pyrene	<MDL	N.D.	<MDL	N.D.	<MDL	N.D.	<MDL	N.D.	N.D.	N.D.	N.D.	N.D.	<MDL	N.D.	N.D.	N.D.	<MQL	N.D.
Benzo[ghi]perylene	<MDL	<MDL	<MDL	<MDL	<MDL	<MDL	<MDL	<MDL	N.D.	N.D.	<MDL	<MQL	<MQL	<MDL	<MDL	<MDL	<MQL	<MDL

715

716 S.I. 15: Concentration (pg m⁻³) of oxy-PAHs in the gas phase measured from 2017 to 2021 at the Princess Elisabeth Station, Antarctica

Sample start	13/12/17	20/12/17	27/12/17	03/01/18	10/01/18	17/01/18	25/01/18	06/02/18	01/12/18	08/12/18	17/12/18	01/01/19	08/01/19	17/01/19
Sample stop	20/12/17	27/12/17	03/01/18	10/01/18	17/01/18	25/01/18	01/02/18	09/02/18	08/12/18	15/12/18	24/12/18	08/01/19	17/01/19	24/01/19
Napthalene-1,4-dione	<MQL	1.07	N.D.	0.49	<MQL	<MQL	N.D.	N.D.	<MQL	<MDL	<MQL	<MDL	<MDL	<MQL
Napthalene-1-carboxaldehyde	8.29	18.92	N.D.	11.74	19.8	14.99	N.D.	1.22	1.83	2.35	8.59	1.26	1.44	7.34
Fluorene-9-one	10.14	13.8	6.11	10.83	7.34	5.5	12.78	6.8	16.5	5.23	7.59	4.99	4.22	9.07
Fluorene-2-carboxaldehyde	N.D.	N.D.	N.D.	N.D.	N.D.	N.D.	N.D.	N.D.	N.D.	N.D.	N.D.	N.D.	N.D.	N.D.
Anthracene-9-one	N.D.	N.D.	N.D.	N.D.	N.D.	N.D.	N.D.	N.D.	N.D.	N.D.	N.D.	N.D.	N.D.	N.D.
Anthracene-9,10-dione	1.06	2.33	1.7	2.93	1.43	1.14	1.52	2.46	1.32	1.61	2.71	1.08	1.34	3.04
2-Methylanthraquinone	<MQL	0.17	<MQL	0.27	<MQL	<MQL	<MQL	<MQL	0.28	<MQL	<MQL	N.D.	N.D.	N.D.
1,8-napthalic anhydride	2.56	17.1	6.47	4.31	7.04	8.72	2.39	2.58	7.87	2.24	3.74	1.22	1.33	3.34
Phenanthrene-9-carboxaldehyde	2.36	10.47	8.75	9.41	6.18	4.57	6.44	5.98	10.01	8.72	12.47	5.52	7.31	9.04
Benzanthrone	N.D.	N.D.	N.D.	N.D.	N.D.	N.D.	N.D.	N.D.	N.D.	N.D.	N.D.	N.D.	N.D.	N.D.
Pyrene-1-carboxaldehyde	N.D.	N.D.	N.D.	N.D.	N.D.	N.D.	N.D.	N.D.	N.D.	N.D.	N.D.	N.D.	N.D.	N.D.
Benz[<i>a</i>]anthracene-7,12-dione	N.D.	N.D.	N.D.	N.D.	N.D.	N.D.	N.D.	N.D.	N.D.	N.D.	N.D.	N.D.	N.D.	N.D.
5,12-Naphthacenequinone	N.D.	N.D.	N.D.	N.D.	N.D.	N.D.	N.D.	N.D.	N.D.	N.D.	N.D.	N.D.	N.D.	N.D.

Sample start	27/11/19	04/12/19	11/12/19	18/12/19	25/12/19	01/01/20	08/01/20	15/01/20	22/01/20	29/01/20	07/12/20	15/12/20	23/12/20	31/12/20	08/01/21	15/01/21	22/01/21	29/01/21
Sample stop	04/12/19	11/12/19	18/12/19	25/12/19	01/01/20	08/01/20	15/01/20	22/01/20	29/01/20	05/02/20	15/12/20	23/12/20	30/12/20	08/01/21	15/01/21	22/01/21	29/01/21	05/02/21
Napthalene-1,4-dione	<MQL	<MDL	<MDL	<MQL	<MDL	<MQL	<MDL	<MQL	<MQL	<MQL	<MDL	<MDL	<MDL	<MDL	<MDL	<MDL	<MDL	<MDL
Napthalene-1-carboxaldehyde	2.19	0.78	1.74	2.46	0.95	3.4	1.2	2.94	4.04	1.19	0.55	2.2	1.65	3.22	3.58	1.3	0.34	1.19
Fluorene-9-one	6	2.89	5.39	5.05	2.99	4.18	3.38	4.76	4.92	3.17	2.12	5.46	4.04	14.44	4	2.98	<MQL	3.16
Fluorene-2-carboxaldehyde	N.D.	N.D.	N.D.	N.D.	N.D.	N.D.	N.D.	N.D.	N.D.	N.D.	N.D.	N.D.	N.D.	N.D.	N.D.	N.D.	N.D.	N.D.
Anthracene-9-one	N.D.	N.D.	N.D.	N.D.	N.D.	N.D.	N.D.	N.D.	N.D.	N.D.	N.D.	N.D.	N.D.	N.D.	N.D.	N.D.	N.D.	N.D.
Anthracene-9,10-dione	0.66	0.61	0.75	1.23	0.77	1.62	0.71	1.25	1.11	0.75	0.51	1.47	0.72	0.9	<MQL	0.6	<MQL	1.02
2-Methylanthraquinone	N.D.	N.D.	N.D.	N.D.	N.D.	N.D.	N.D.	N.D.	N.D.	N.D.	N.D.	N.D.	N.D.	N.D.	N.D.	<MDL	N.D.	<MQL
1,8-napthalic anhydride	0.77	0.58	0.87	1.16	0.67	4.57	0.55	<MQL	0.94	0.63	0.62	<MQL	<MQL	N.D.	N.D.	<MQL	<MQL	<MDL
Phenanthrene-9-carboxaldehyde	10.35	13.64	13.37	23.84	10.19	18.82	12.35	18.69	13.42	12.86	13.89	26.82	18.06	8.22	11.38	9.05	9.96	14.44
Benzanthrone	N.D.	N.D.	N.D.	N.D.	N.D.	N.D.	N.D.	N.D.	N.D.	N.D.	N.D.	N.D.	N.D.	N.D.	N.D.	N.D.	N.D.	N.D.
Pyrene-1-carboxaldehyde	N.D.	N.D.	N.D.	N.D.	N.D.	N.D.	N.D.	N.D.	N.D.	N.D.	N.D.	N.D.	N.D.	N.D.	N.D.	N.D.	N.D.	N.D.
Benz[<i>a</i>]anthracene-7,12-dione	N.D.	N.D.	N.D.	N.D.	N.D.	N.D.	N.D.	N.D.	N.D.	N.D.	N.D.	N.D.	N.D.	N.D.	N.D.	N.D.	N.D.	N.D.
5,12-Naphthacenequinone	N.D.	N.D.	N.D.	N.D.	N.D.	N.D.	N.D.	N.D.	N.D.	N.D.	N.D.	N.D.	N.D.	N.D.	N.D.	N.D.	N.D.	N.D.

717

718 S.I. 16: Concentration (pg m⁻³) of oxy-PAHs in the particle phase measured from 2017 to 2021 at the Princess Elisabeth Station, Antarctica

Sample start	13/12/17	20/12/17	27/12/17	03/01/18	10/01/18	17/01/18	25/01/18	06/02/18	01/12/18	08/12/18	17/12/18	01/01/19	08/01/19	17/01/19
Sample stop	20/12/17	27/12/17	03/01/18	10/01/18	17/01/18	25/01/18	01/02/18	09/02/18	08/12/18	15/12/18	24/12/18	08/01/19	17/01/19	24/01/19
Napthalene-1,4-dione	0.06	0.29	1.04	0.42	0.24	N.D.	0.17	N.D.	N.D.	0.19	0.16	N.D.	0.11	N.D.
Napthalene-1-carboxaldehyde	0.42	1.43	0.82	1.41	0.81	0.3	0.29	<MQL	N.D.	<MQL	<MQL	<MQL	<MDL	0.53
Fluorene-9-one	1.7	1.41	1.36	1.55	1.96	1.55	1.54	2.55	1.46	1.39	1.3	<MQL	<MQL	2
Fluorene-2-carboxaldehyde	N.D.	N.D.	N.D.	N.D.	N.D.	N.D.	N.D.	N.D.	N.D.	N.D.	N.D.	N.D.	N.D.	N.D.
Anthracene-9-one	N.D.	N.D.	N.D.	N.D.	0.12	0.17	N.D.	N.D.	N.D.	N.D.	N.D.	N.D.	N.D.	N.D.
Anthracene-9,10-dione	7.81	14.57	4.34	5.71	3.96	3.76	7.09	5.5	6.71	3.03	2.52	1.56	1.4	1.2
2-Methylanthraquinone	1.98	2.25	1.09	2.01	2.43	1.49	2.3	1.99	1.87	1.1	0.87	0.69	0.73	0.54
1,8-napthalic anhydride	3.46	26.77	9.93	16.53	8.23	5.63	6.46	8.92	4.48	4.03	7.62	5.54	5.43	3.44
Phenanthrene-9-carboxaldehyde	N.D.	N.D.	<MDL	N.D.	N.D.	N.D.	N.D.	N.D.	N.D.	<MDL	<MDL	<MDL	<MDL	<MDL
Benzanthrone	0.3	2.22	0.71	0.5	0.5	0.62	0.15	0.17	0.08	0.06	0.18	0.07	<IDL	0.1
Pyrene-1-carboxaldehyde	<IDL	0.14	<IDL	N.D.	N.D.	N.D.	N.D.	N.D.	N.D.	N.D.	N.D.	N.D.	N.D.	N.D.
Benz[<i>a</i>]anthracene-7,12-dione	0.2	1.28	0.53	0.34	0.23	0.39	0.12	N.D.	N.D.	N.D.	N.D.	N.D.	N.D.	N.D.
5,12-Naphthacenequinone	N.D.	0.25	0.24	<IDL	N.D.	<IDL	N.D.	N.D.	N.D.	N.D.	N.D.	N.D.	N.D.	N.D.

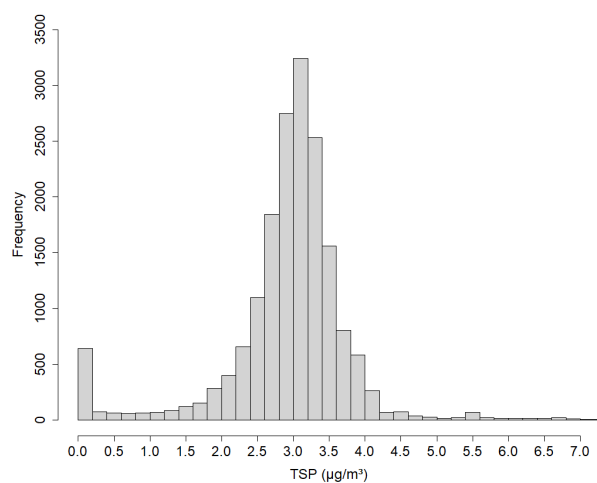
Sample start	27/11/19	04/12/19	11/12/19	18/12/19	25/12/19	01/01/20	08/01/20	15/01/20	22/01/20	29/01/20	07/12/20	15/12/20	23/12/20	31/12/20	08/01/21	15/01/21	22/01/21	29/01/21
Sample stop	04/12/19	11/12/19	18/12/19	25/12/19	01/01/20	08/01/20	15/01/20	22/01/20	29/01/20	05/02/20	15/12/20	23/12/20	30/12/20	08/01/21	15/01/21	22/01/21	29/01/21	05/02/21
Napthalene-1,4-dione	N.D.	N.D.	0.15	0.18	<IDL	0.07	N.D.	N.D.	0.15	N.D.	0.18	0.28	0.25	N.D.	0.2	0.11	0.77	0.23
Napthalene-1-carboxaldehyde	<MDL	<MQL	<MDL	0.45	<MDL	<MQL	<MQL	<MQL	0.58	<MDL	<MQL	<MDL	0.9	N.D.	<MQL	<MDL	0.75	<MQL
Fluorene-9-one	1.41	<MQL	<MQL	1.78	<MQL	<MQL	<MQL	<MQL	<MQL	<MQL	1.31	4.04	3.65	4.48	2.68	1.14	2.27	2.18
Fluorene-2-carboxaldehyde	N.D.	N.D.	N.D.	N.D.	N.D.	N.D.	N.D.	N.D.	N.D.	N.D.	N.D.	N.D.	N.D.	N.D.	N.D.	N.D.	N.D.	N.D.
Anthracene-9-one	0.35	N.D.	N.D.	N.D.	N.D.	N.D.	0.1	N.D.	N.D.	N.D.	N.D.	N.D.	N.D.	N.D.	N.D.	N.D.	N.D.	N.D.
Anthracene-9,10-dione	2.56	1.24	1.36	<MQL	<MQL	<MQL	1.02	<MQL	<MQL	<MQL	0.84	<MQL	1.61	4.25	1.69	1.17	1.87	<MQL
2-Methylanthraquinone	0.68	0.54	0.45	0.34	0.29	<IDL	0.29	0.35	<IDL	<IDL	0.22	<IDL	0.46	0.45	<IDL	0.23	0.57	<IDL
1,8-napthalic anhydride	5.77	6.41	5.73	6.29	4.25	0.34	2.87	2.67	3.07	2.4	3.49	2.82	3	5	2.22	2.26	3.98	1.22
Phenanthrene-9-carboxaldehyde	N.D.	N.D.	N.D.	<MDL	N.D.	<MDL	N.D.	N.D.	N.D.	N.D.	<MDL	<MDL	<MDL	N.D.	<MDL	N.D.	<MQL	N.D.
Benzanthrone	0.1	0.07	0.06	<IDL	0.06	0.06	N.D.	<IDL	N.D.	<IDL	N.D.	N.D.	0.16	N.D.	N.D.	N.D.	0.46	N.D.
Pyrene-1-carboxaldehyde	N.D.	N.D.	N.D.	N.D.	N.D.	<IDL	N.D.	N.D.	N.D.	N.D.	N.D.	N.D.	N.D.	N.D.	N.D.	N.D.	N.D.	N.D.
Benz[<i>a</i>]anthracene-7,12-dione	N.D.	N.D.	N.D.	N.D.	N.D.	N.D.	N.D.	N.D.	N.D.	N.D.	N.D.	N.D.	N.D.	N.D.	N.D.	N.D.	N.D.	N.D.
5,12-Naphthacenequinone	N.D.	N.D.	N.D.	N.D.	N.D.	N.D.	N.D.	N.D.	N.D.	N.D.	N.D.	N.D.	N.D.	N.D.	N.D.	N.D.	N.D.	N.D.

719

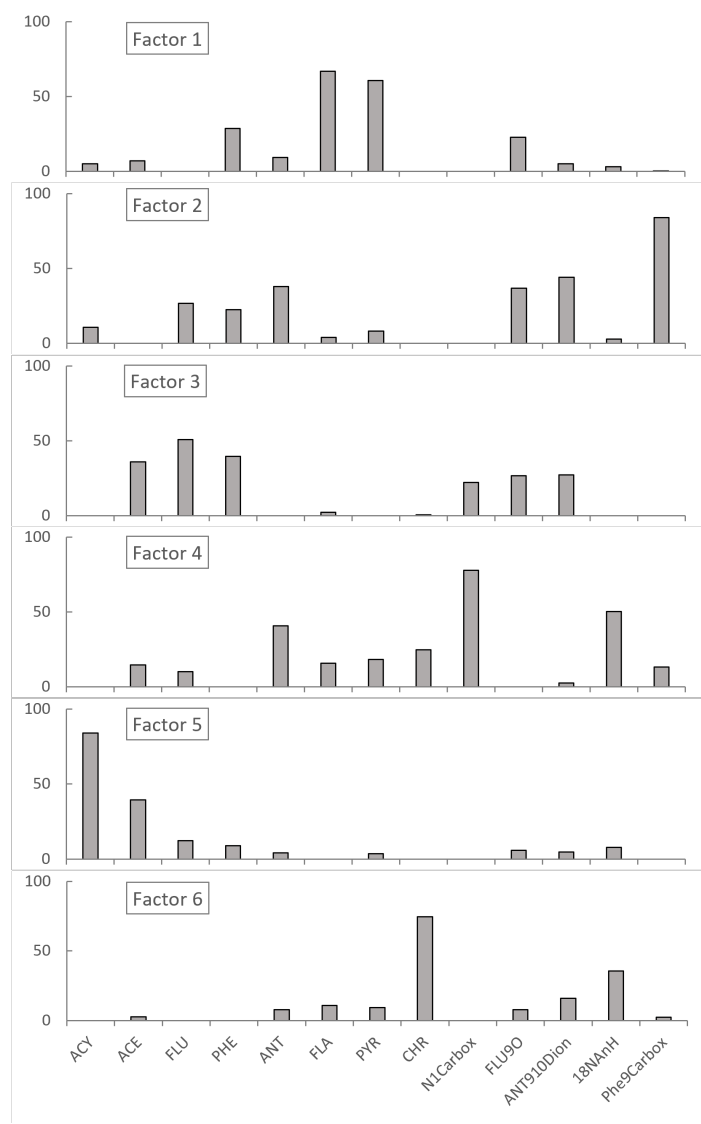
720

S.I. 17: Method Detection Limit (MDL) and Method Quantification Limit (MQL) given as a range of air concentrations under standard conditions and both sample media types. MDL and MQL depend on the sample volume. For samples for which no signal was detected in the field blanks the Instrumental Detection Limit (IDL) was used instead.

	PUF		QFF	
	MDL pg m ⁻³	MQL pg m ⁻³	MDL pg m ⁻³	MQL pg m ⁻³
Naphthalene	3.2-16.3	6.7-33.9	-	-
Acenaphthylene	IDL	IDL	IDL	IDL
Acenaphthene	0.1-0.7	0.3-1.4	IDL	IDL
Fluorene	0.2-1.2	0.4-2.2	0.1-0.5	0.1-0.7
Phenanthrene	0.5-2.3	0.7-3.6	0.2-1.3	0.4-2.3
Anthracene	0.1-0.5	0.1-0.7	IDL	IDL
Fluoranthene	0.1-0.7	0.2-1	0.1-0.3	0.1-0.5
Pyrene	0.2-0.9	0.4-1.8	0-0.2	0.1-0.3
Benz[<i>a</i>]anthracene	0.4-1.8	1-4.8	IDL	IDL
Chrysene	IDL	IDL	IDL	IDL
Benzo[<i>b</i>]fluoranthene	0.1-0.4	0.2-1.1	0.1-0.4	0.2-0.9
Benzo[<i>k</i>]fluoranthene	0.1-0.4	0.2-1	0.1-0.4	0.2-0.9
Benzo[<i>a</i>]pyrene	0-0.2	0.1-0.5	IDL	IDL
Dibenz[<i>a,h</i>]anthracene	0.2-0.8	0.4-2	0.1-0.3	0.2-0.8
Indeno[1,2,3- <i>cd</i>]pyrene	0.1-0.4	0.2-0.8	0.1-0.3	0.1-0.7
Benzo[<i>ghi</i>]perylene	0.1-0.5	0.2-0.9	0.1-0.4	0.2-0.8
Napthalene-1,4-dione	0.1-0.7	0.3-1.6	IDL	IDL
Napthalene-1-carboxaldehyde	0.1-0.4	0.1-0.7	0.1-0.3	0.1-0.7
Fluorene-9-one	0.7-3.5	1.1-5.3	0.4-1.9	0.6-3
Fluorene-2-carboxaldehyde	IDL	IDL	IDL	IDL
Anthracene-9-one	0.2-1	0.4-2.2	IDL	IDL
Anthracene-9,10-dione	0.2-0.8	0.3-1.3	0.2-1	0.4-2.2
2-Methylantraquinone	0-0.2	0.1-0.5	IDL	IDL
1,8-napthalic anhydride	0.2-1	0.3-1.6	0.1-0.6	0.1-0.7
Phenanthrene-9-carboxaldehyde	0.3-1.8	0.9-4.6	0.1-0.6	0.2-1.2
Benzanthrone	IDL	IDL	IDL	IDL
Pyrene-1-carboxaldehyde	IDL	IDL	IDL	IDL
Benz[<i>a</i>]anthracene-7,12-dione	IDL	IDL	IDL	IDL
5,12-Naphthacenequinone	IDL	IDL	IDL	IDL



S.I. 18: Histogram of the TEOM-FDMS data for the summer of 2018-19, 2019-20 and 2020-21



S.I. 19: Profiles expressed as the percentage of the sum of the compound of the 6 factors as determined by the PMF model.